

Review

# Transition Metal Dichalcogenides Nanoscrolls: Preparation and Applications

Shilong Yu, Pinyi Wang, Huihui Ye, Hailun Tang, Siyuan Wang, Zhikang Wu, Chengjie Pei, Junhui Lu and Hai Li \*

Key Laboratory of Flexible Electronics (KLOFE) & Institute of Advanced Materials (IAM), Nanjing Tech University, Nanjing 211816, China

\* Correspondence: iamhli@njtech.edu.cn

**Abstract:** Two-dimensional (2D) transition metal dichalcogenides (TMDCs) nanosheets have shown extensive applications due to their excellent physical and chemical properties. However, the low light absorption efficiency limits their application in optoelectronics. By rolling up 2D TMDCs nanosheets, the one-dimensional (1D) TMDCs nanoscrolls are formed with spiral tubular structure, tunable interlayer spacing, and opening ends. Due to the increased thickness of the scroll structure, the light absorption is enhanced. Meanwhile, the rapid electron transportation is confined along the 1D structure. Therefore, the TMDCs nanoscrolls show improved optoelectronic performance compared to 2D nanosheets. In addition, the high specific surface area and active edge site from the bending strain of the basal plane make them promising materials for catalytic reaction. Thus, the TMDCs nanoscrolls have attracted intensive attention in recent years. In this review, the structure of TMDCs nanoscrolls is first demonstrated and followed by various preparation methods of the TMDCs nanoscrolls. Afterwards, the applications of TMDCs nanoscrolls in the fields of photodetection, hydrogen evolution reaction, and gas sensing are discussed.

**Keywords:** TMDCs; nanosheet; nanoscroll; preparation; photodetection; hydrogen evolution reaction; gas sensing



**Citation:** Yu, S.; Wang, P.; Ye, H.; Tang, H.; Wang, S.; Wu, Z.; Pei, C.; Lu, J.; Li, H. Transition Metal Dichalcogenides Nanoscrolls: Preparation and Applications. *Nanomaterials* **2023**, *13*, 2433. <https://doi.org/10.3390/nano13172433>

Academic Editor: Andrey Chuvalin

Received: 20 July 2023

Revised: 21 August 2023

Accepted: 25 August 2023

Published: 27 August 2023



**Copyright:** © 2023 by the authors. Licensee MDPI, Basel, Switzerland. This article is an open access article distributed under the terms and conditions of the Creative Commons Attribution (CC BY) license (<https://creativecommons.org/licenses/by/4.0/>).

## 1. Introduction

As representative two-dimensional (2D) materials, the transition metal dichalcogenides (TMDCs) nanosheets have been successfully applied in the fields of photodetection [1–6], energy storage [7–11], catalysis [12–16], and so on. Although the monolayer TMDCs nanosheets have shown excellent optoelectronic performance, their low light absorption efficiency hinders the applications in photodetection [17], because of their ultrathin thickness.

A great deal of effort has been developed to improve the light absorption of TMDCs nanosheets, such as plasma treatment, formation of van der Waals heterojunction, utilization of plasmonic effect, integration of quantum dots [18–22], etc. Recently, rolling up the monolayer TMDCs nanosheet to form the TMDCs nanoscroll (TMDCs-NS) has been reported as a promising method to improve their optoelectronic performance [19]. With the aid of volatile organic solvents or alkaline solution [19,23–27], the monolayer TMDCs nanosheets can be transformed into one-dimensional (1D) nanoscrolls with tubular and spiral structures [23,28,29]. The as-obtained TMDCs nanoscroll (TMDCs-NS) showed enhanced light absorption due to the increased cross-section. In addition, the TMDCs-NS also inherits the excellent properties from the monolayer TMDCs nanosheet [21,30–35]. Furthermore, the curved structure of the nanoscroll exhibits strain, which can modulate the band gap of TMDCs nanosheet [33]. Moreover, its scrolled structure has tunable interlayer space with open ends, in which other functional nanomaterials can be encapsulated [35,36]. Therefore, the TMDCs-NS have attracted great attention in optoelectronics in recent years.

In this review, we introduce the structure, fabrication, and applications of TMDCs-NS. Firstly, the structure of nanoscrolls is demonstrated. Secondly, the preparation methods of nanoscrolls are discussed in detail. We then present the applications of TMDCs-NS in the photodetection, sensing, and hydrogen evolution reaction.

## 2. Structure of TMDCs-NS

Different from other 1D nanomaterials, the nanoscrolls have spiral tubular structure with weak van der Waals (vdW) interaction between adjacent layers, which are transformed from 2D nanosheet, exhibiting open ends and side edges without fusion as shown in Figure 1b. To date, various 2D nanosheets can be transformed into nanoscrolls, such as graphene, TMDCs, black phosphorus and h-BN [37–42]. The graphene nanoscroll was discovered in the arc discharge experiment of graphite electrode [43], and confirmed by transmission electron microscopy (TEM) [44]. The large-scale preparation of graphene nanoscroll was proposed in 2003 and then received much attention [45,46].

Similar to graphene nanoscroll, the TMDCs-NS is also composed of monolayer TMDCs nanosheets scrolled up into Archimedean helical structure (Figure 1c) [37,47]. These TMDCs-NS have unique physical and chemical properties due to their nanoscale dimensions and high surface area-to-volume ratio, which make them useful in a variety of applications, such as energy storage, catalysis, and optoelectronics [19,27,48–52].

The structure of TMDCs-NS is illustrated by taking MoS<sub>2</sub> nanoscroll as an example. By scrolling a monolayer MoS<sub>2</sub> nanosheet (Figure 1a), the MoS<sub>2</sub> nanoscroll is formed with an inner layer radius of  $R_{in}$ , an outer layer radius of  $R_{out}$ , and a interlayer spacing of  $h$ , as shown in Figure 1c [53–55]. The scrolling direction is usually along the armchair or zigzag orientation of the MoS<sub>2</sub> nanosheet (Figure 1d) [53]. A molecular dynamics (MD) simulation was performed to understand the scrolling direction of MoS<sub>2</sub> at the molecular level (Figure 1e). The results indicate that the energy per atom of nanoscrolls along the armchair orientation is lower than those of nanoscrolls through the zigzag and chiral orientations (Figure 1f). As a consequence, the armchair orientation (Mo-S bond direction) is the dominant trend to roll up the MoS<sub>2</sub> nanosheet into MoS<sub>2</sub> nanoscrolls [56]. The spacing between adjacent layers of MoS<sub>2</sub> nanoscroll also plays an important role in determining its stability. As the interlayer spacing increases from 4 to 5.5 Å, the energy of each atom decreases quickly (Figure 1g). While it increases continuously as the interlayer spacing increases from 5.5 to 10 Å. The MoS<sub>2</sub> nanoscroll is in an energy-favorable state when the interlayer spacing is in the range of 4.7~6.5 Å [47,53].

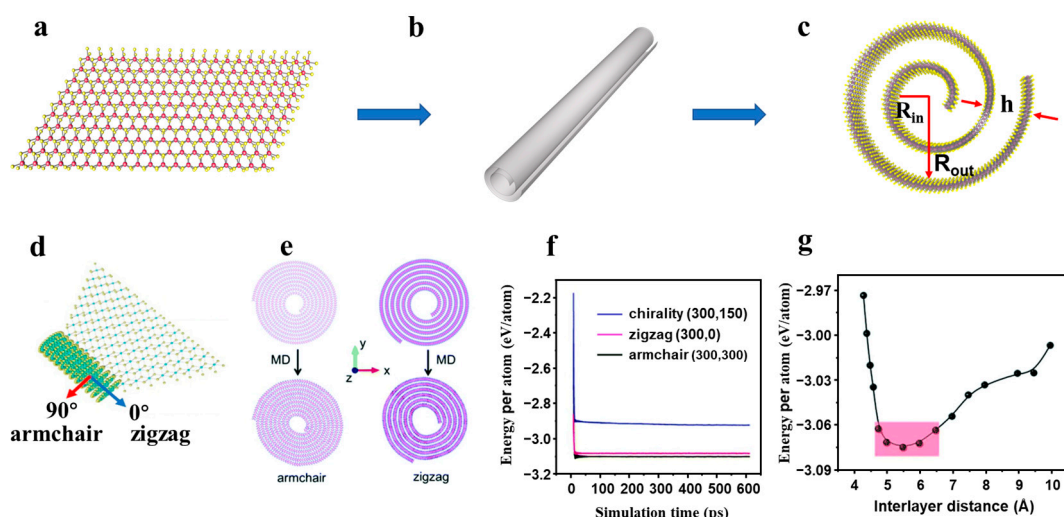


**Figure 1.** (a) Monolayer MoS<sub>2</sub> nanosheet. (b) Schematic structure of the TMDCs nanoscroll with open ends and side edges. (c) The MoS<sub>2</sub> nanoscroll with inter-core radius  $R_{in}$ , outer radius  $R_{out}$  and

interlayer spacing  $h$ . (d) The formation of the  $\text{MoS}_2$  nanoscrolls are always along the armchair direction (Mo–S bond direction) [56]. (e) The  $\text{MoS}_2$  sheets of the same size roll through the armchair (left) and zigzag (right) orientation molecular dynamics (MD) simulations before (upper) and after (lower) structural relaxation [53]. (f) The relationship between unit atomic energy and simulation time of  $\text{MoS}_2$  nanoscrolls with armchair, zigzag, and chiral orientation [53]. (g) The atomic energy is a function of  $\text{MoS}_2$  nanoscroll spacing. The red area indicates the energy-favorable interlayer distance [53].

### 3. Preparation of TMDCs Nanoscrolls

In recent years, many TMDCs nanosheets have been reported to form TMDCs-NS, including  $\text{MoS}_2$ ,  $\text{WS}_2$ ,  $\text{MoSe}_2$ ,  $\text{MoS}_2/\text{WS}_2$ , etc. [3,9,17–20,29,33,51–53,57–68]. Several methods have been successfully developed to prepare TMDCs-NS, such as strain-induced scrolling [17], argon plasma-assisted scrolling [18], supercritical fluid-assisted scrolling [68,69], volatile organic solvent-induced scrolling [23–25,33,70], alkaline droplet assisted scrolling [19,21,26,27,35], and vortex flow device (VFD) induced continuous flow [50].

Theoretical investigation indicates that there is an energy barrier between the nanosheet and nanoscroll [71–73]. A driving activation energy is required to initialize the scrolling automatically [74]. By scrolling or folding the nanosheet into a nanoscroll, the lowest energy form is presented [74]. The barrier can be overcome with the help of external force in liquid or in air, where the TMDCs-NS is formed.

#### 3.1. Fabrication of TMDCs Nanoscrolls in Liquid

##### 3.1.1. Solvent Evaporation to Make Nanoscrolls

Many organic solvents are liquid at ambient conditions with large volatility, which can be used to assist or induce the scrolling of TMDCs nanosheets [23,33,35,75–77], such as acetone, ethanol, and isopropanol [24,78–80]. In 2018, we proposed the preparation of  $\text{MoS}_2$  nanoscroll by dropping an ethanol or acetone droplet on monolayer  $\text{MoS}_2$  nanosheet [23], as shown in Figure 2. Monolayer  $\text{MoS}_2$  nanosheets were first obtained by chemical vapor deposition (CVD) on  $\text{SiO}_2/\text{Si}$  (Figure 2a,b), and a drop of ethanol was deposited on the  $\text{MoS}_2$  nanosheets (Figure 2c). Due to its low surface tension, the ethanol can wet  $\text{MoS}_2$  and  $\text{SiO}_2/\text{Si}$  substrates easily. During the evaporation process, a thin ethanol layer is formed near the contact line (Figure 2d). With the rapid evaporation of ethanol, a temperature gradient is generated near the contact line, creating a surface tension gradient to induce fluid flow. Such kind of fluid flow could roll up the edge of  $\text{MoS}_2$ . As the contact line moves, the  $\text{MoS}_2$  nanosheet continues to be rolled up until a complete  $\text{MoS}_2$  nanoscroll is formed (Figure 2e) [23].

By dropping the mixture of ethanol and water on CVD-grown monolayer  $\text{MoS}_2$  nanosheet, Jian Zheng et al. also successfully prepared  $\text{MoS}_2$  nanoscrolls, as shown in Figure 3 [24]. Large-area monolayer  $\text{MoS}_2$  nanosheets were obtained firstly by CVD (Figure 3a).  $\text{MoS}_2$  nanoscrolls were then fabricated in a short time in a mixture solution of ethanol and water with a volume ratio of 2:1 (ethanol:water = 2:1).

Due to the high temperature-causing mismatch between the  $\text{MoS}_2$  nanosheet and substrate during CVD growth (Figure 3a), a strain equilibrium is balanced between them when the temperature decreases to room temperature (Figure 3b). When the mixture solution is dropped onto the  $\text{MoS}_2$  nanosheet, the ethanol intercalates between the  $\text{MoS}_2$  and substrate, and the upper part of  $\text{MoS}_2$  is detached from the substrate. In this case, the strain balance is broken (Figure 3c), and the released portion curls into a roll (Figure 3d). Due to the adhesion from the substrate, the left portion remains intact [24]. With the evaporation of ethanol, the surface tension at the air-solvent- $\text{MoS}_2$  interface is greater than that between  $\text{MoS}_2$  and the substrate. As a result, the strain-adhesion balance is broken continuously, generating  $\text{MoS}_2$  nanoscroll finally (Figure 3e).

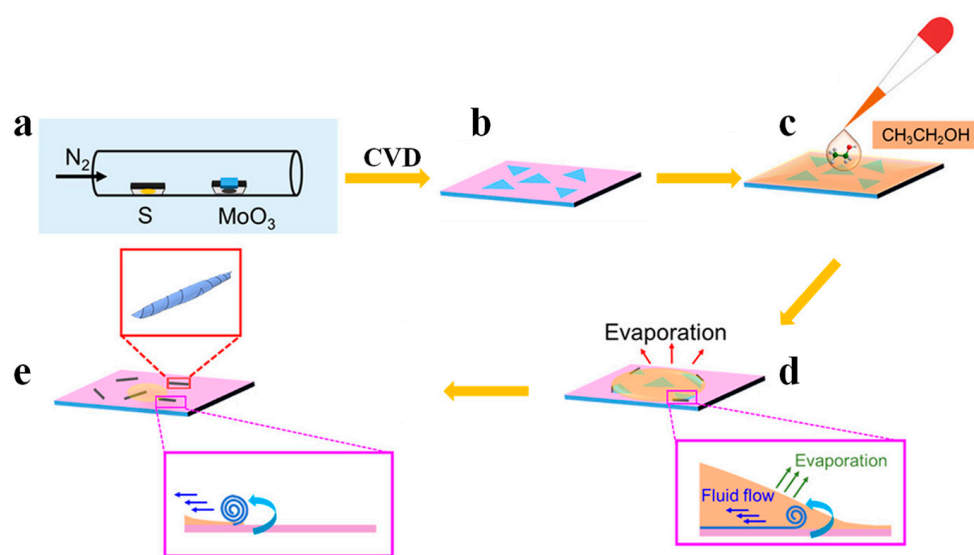


**Figure 2.** Volatile organic solvent-assisted fabrication of MoS<sub>2</sub> nanoscroll [23]. (a,b) CVD growth of monolayer MoS<sub>2</sub> nanosheets. (c) A drop of ethanol is deposited on MoS<sub>2</sub> nanosheets. (d) The edges of MoS<sub>2</sub> nanosheets are rolled up during the evaporation of ethanol. (e) MoS<sub>2</sub> nanoscrolls were formed.

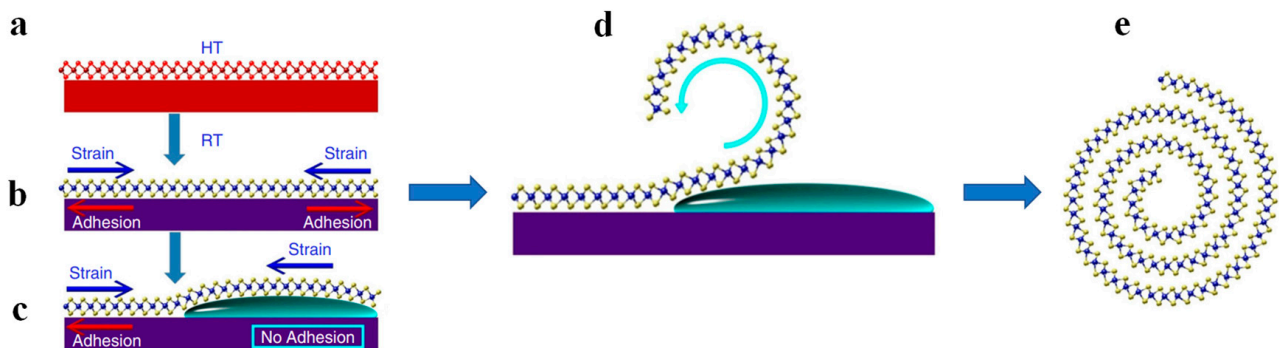


**Figure 3.** The mixture of ethanol and water-assisted fabrication of MoS<sub>2</sub> nanoscroll [24]. (a) CVD growth of MoS<sub>2</sub> nanosheet. (b) Strain-balanced MoS<sub>2</sub> on substrate. (c) After ethanol intercalation, the strain-adhesion balance between MoS<sub>2</sub> and substrate is broken. (d) Rolling up the edge of the MoS<sub>2</sub> nanosheet. (e) The as-prepared MoS<sub>2</sub> nanoscroll.

### 3.1.2. Alkaline Droplet-Assisted Fabrication of Nanoscrolls

For bilayer and multilayer nanosheets, it is difficult to roll them up effectively due to the strong adhesion force from the substrate. Since TMDCs nanosheets are usually grown on SiO<sub>2</sub>/Si substrate, etching the SiO<sub>2</sub> layer beneath them could eliminate the strong adhesion from the substrate. Therefore, alkaline solution has been used to etch the SiO<sub>2</sub> layer, and thus break the adhesion energy between the nanosheet and substrate (Figure 4). As a result, the strain equilibrium is broken, rolling up the TMDCs nanosheet from edges to form spiral nanoscrolls [19,51].

The materials for fabricating nanoscrolls are derived from 2D nanosheets produced by mechanical stripping [78] or CVD. The experiments were dominated by CVD-prepared nanosheets, but the nanosheets prepared by CVD in most cases are accompanied by the production of defects, homojunctions, and heterojunctions [81]. Therefore, we successfully fabricated nanoscrolls using CVD-prepared heterojunction nanosheets. In 2020, we proposed a method to scroll the MoS<sub>2</sub>/WS<sub>2</sub> heterostructure nanosheet by using an alkaline solution. Firstly, large-area MoS<sub>2</sub>/WS<sub>2</sub> heterostructure nanosheets were grown on SiO<sub>2</sub>/Si substrate by CVD (Figure 4a) [19,81]. Afterwards, 50 μL of alkaline aqueous solution (0.1 M KOH or NaHCO<sub>3</sub>) was dropped on the nanosheets. The SiO<sub>2</sub> layer was etched by the

alkaline solution, allowing penetration of the alkaline solution into the interface of the nanosheet and  $\text{SiO}_2/\text{Si}$  substrate (Figure 4b), which could further etch the  $\text{SiO}_2$  layer to release the edge of the nanosheet. To decrease the energy form, the released edge of the nanosheet tends to be scrolled (Figure 4c). With the further etching of the  $\text{SiO}_2$  layer, more portions of the nanosheet were released and continuously scrolled till forming nanoscroll (Figure 4c,d) [19]. The as-obtained nanoscroll was then rinsed with deionized (DI) water and dried with  $\text{N}_2$  for characterization and device fabrication (Figure 4d). Furthermore MoS<sub>2</sub>/WS<sub>2</sub> heterostructures nanosheet, we found that the silver nanoparticles decorated monolayer MoS<sub>2</sub> and WS<sub>2</sub> nanosheets could also be rolled up effectively by using an alkaline solution [35].

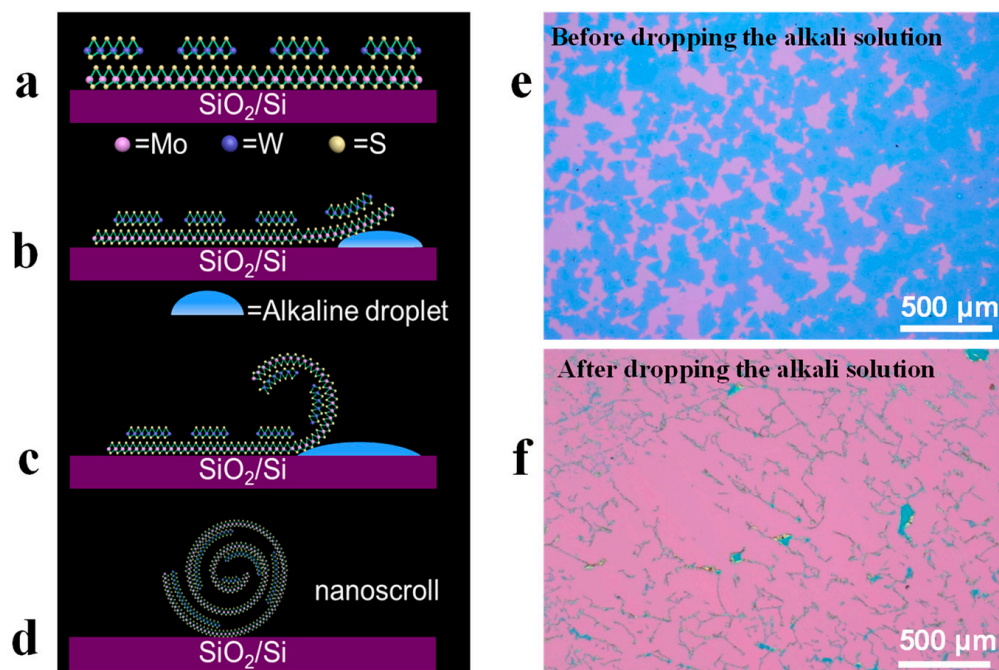


**Figure 4.** Alkaline droplet-assisted fabrication of nanoscrolls [19]. (a) CVD-grown MoS<sub>2</sub>/WS<sub>2</sub> heterostructures nanosheet on SiO<sub>2</sub>/Si substrate. (b) Etching the SiO<sub>2</sub> layer beneath the nanosheet by dropping an alkaline solution. (c) The edge of the WS<sub>2</sub>/MoS<sub>2</sub> nanosheet is rolled up due to the elimination of strong adhesion from the substrate. (d) The as-formed WS<sub>2</sub>/MoS<sub>2</sub> heterojunction nanoscroll. (e,f) Show the comparison before and after dropping the alkali solution on the MoS<sub>2</sub>/WS<sub>2</sub> nanosheets.

Duan et al. found that 80% of the bilayer and trilayer TMDCs heterostructure nanosheets could be transformed into 1D nanoscrolls by using a mixture of ethanol and water. However, many scrolls are incompletely rolled up with tightly pinned edges, indicating the mixed solvent does not work well to completely delaminate the edges of a thick 2D nanosheet. The yield of the nanoscroll increased to 90% by adding 5% ammonia into the mixed solvent, with 60% of them showing a closely stacked scroll structure. The result indicated that the etching of the SiO<sub>2</sub> layer by alkaline solution played an important role in peeling off the 2D nanosheet from the substrate even the existence of strong edge-substrate interaction [21,24].

Similarly, alkaline solution was also employed to roll up PbI<sub>2</sub>/MoS<sub>2</sub> and BaTiO<sub>3</sub>/MoS<sub>2</sub> nanosheets into complete nanoscroll, further confirming the importance of alkaline solution in preparation of TMDCs-NS [3,27,51].

### 3.1.3. Fabrication of TMDCs Nanoscrolls by Dragging Water Droplets

Due to the low surface tension of organic solvent, it is easily adsorbed on TMDCs nanosheets. Thus, it is inevitable to trap organic solvent in the TMDCs-NS during the scrolling process. It is known that the adsorbed organic solvent could greatly influence

the properties and device performance of TMDCs nanosheets. Therefore, it is desirable to fabricate TMDCs-NS without using organic solvent. Recently, we reported an organic solvent-free method to fabricate tightly-packed TMDCs-NS [52]. Firstly, CVD-grown monolayer MoS<sub>2</sub> nanosheets were heated at 100 °C, as shown in Figure 5a,b. After 3 μL of deionized (DI) water droplet was dropped on the MoS<sub>2</sub> nanosheets (Figure 5c), The coverslips were dragged from one end to the other at a speed of 3 mm/s (Figure 5d). Afterwards, large scale closely packed MoS<sub>2</sub> nanoscrolls were fabricated (Figure 5e).

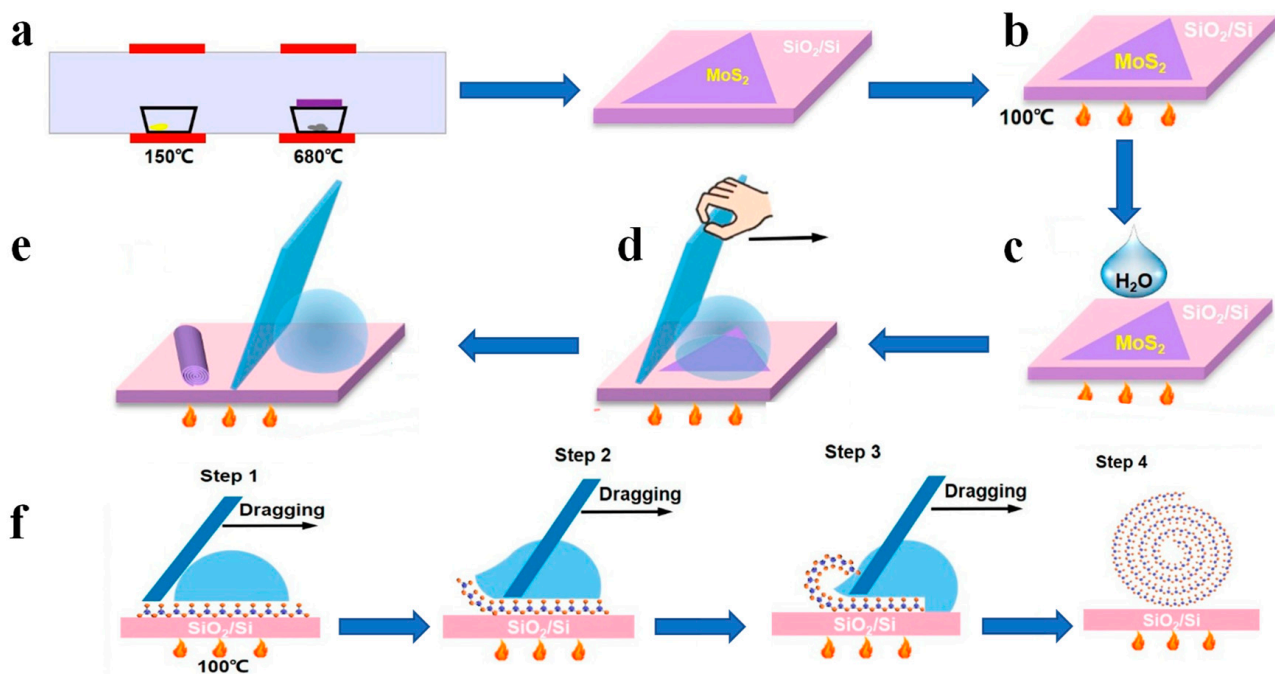


**Figure 5.** Fabrication of TMDCs nanoscrolls by dragging water droplets at 100 °C [52]. (a) Monolayer MoS<sub>2</sub> nanosheet was grown by CVD at 680 °C. (b) Heat the substrate and MoS<sub>2</sub> nanosheets for 10 min. (c) A drop of H<sub>2</sub>O on the MoS<sub>2</sub> film. (d) The H<sub>2</sub>O droplet was dragged across the MoS<sub>2</sub> nanosheet on the SiO<sub>2</sub>/Si substrate by a coverslip at 3 mm/s<sup>-1</sup>; (e) MoS<sub>2</sub> nanoscroll was formed after removing the H<sub>2</sub>O droplet; (f) Schematic diagram of the formation of the MoS<sub>2</sub>-NS.

The detailed mechanism for the formation of nanoscrolls could be explained as follows, as shown in Figure 5f. When the monolayer MoS<sub>2</sub> nanosheets on SiO<sub>2</sub>/Si substrate were heated at 100 °C, the adhesion force between the nanosheets and substrate was weakened. Therefore, with the movement of water droplets, the scrolling occurs first at the edges of MoS<sub>2</sub> nanosheets. Due to the hydrophobicity of MoS<sub>2</sub> nanosheets, the low friction between water and MoS<sub>2</sub> and the high surface tension of water contribute to the following scrolling of MoS<sub>2</sub> nanosheets. More importantly, due to the hydrophobicity of MoS<sub>2</sub>, the water molecules were difficult to trap in the nanoscrolls, obtaining solvent-free and closely packed nanoscrolls [52].

### 3.1.4. Amine-Functional Amphiphilic Molecule Assisted Fabrication of TMDCs Nanoscrolls

The involvement of amphiphilic molecules in the preparation of MoS<sub>2</sub>, MoSe<sub>2</sub>, and MoTe<sub>2</sub> nanoscrolls has also been investigated [48,49,82,83]. By mixing N-(2-aminoethyl)-3α-hydroxy-5β-cholan-24-amide (LCA) and exfoliated TMDCs nanosheets in orthodichlorobenzene (ODCB) for 24 h at room temperature, TMDCs-NS was obtained in large scale (Figure 6a). The formation of MoS<sub>2</sub> nanoscrolls with the help of LCA could be explained as follows. Firstly, the LCA molecules were self-assembled into fibers in ODCB. The amine group of LCA fiber has a stronger interaction with the edges of TMDCs nanosheets than the entire plane. Thus, the edges start scrolling around the LCA fibers. With the gradual

self-assembly of LCA fiber, the interaction of fiber with the edges of TMDCs nanosheets is enhanced. In this case, the original equilibrium state of TMDCs nanosheets is broken and the nanosheet scrolls spontaneously. Therefore, TMDCs-NS was formed. By using this method, MoS<sub>2</sub> nanoscrolls, MoS<sub>2</sub>-Ag nanoparticles nanoscrolls, and MoS<sub>2</sub>-Au nanoparticles nanoscrolls have been successfully prepared [49,83].

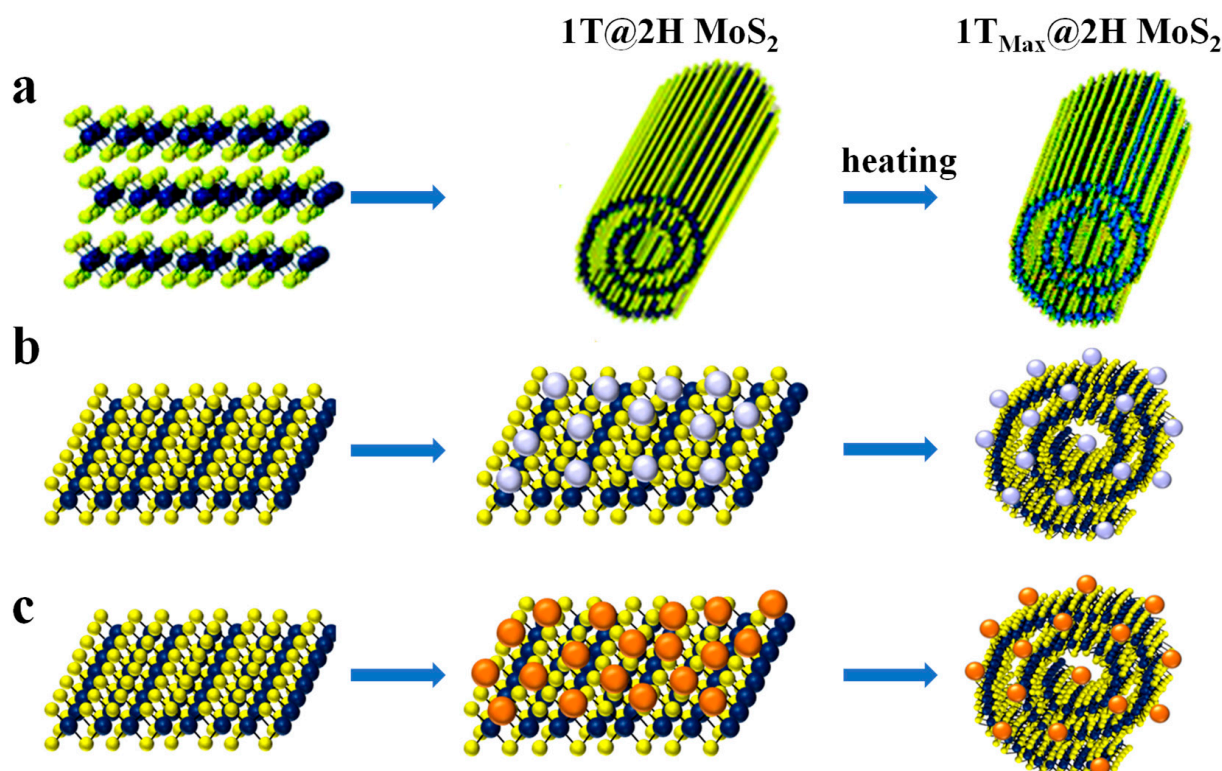


**Figure 6.** Amine-functional amphiphilic molecule assisted fabrication of TMDCs nanoscrolls. (a) Scheme of Amine-functional amphiphilic molecule assisted fabrication of 1T@2H MoS<sub>2</sub> nanoscrolls [49]. (b,c) Scheme of Amine-functional amphiphilic molecule assisted fabrication of MoS<sub>2</sub>-Ag and MoS<sub>2</sub>-Au nanoscrolls [83].

### 3.1.5. Supercritical Fluid-Assisted Fabrication of Nanoscrolls

Supercritical fluids (SCFs) are fluids with much more space and are highly compressible than ordinary fluids above their critical temperatures and pressure [84,85]. By controlling the temperature or pressure, the density and solvent strength of SCFs can be tuned from gas-like to solid-like [49,83,86,87]. SCF has unique properties such as gas diffusivity, liquid solubility, low interfacial tension, excellent surface wettability, and high diffusion coefficient [88–90]. Thus, SCFs processing has been used as a promising and effective route to exfoliate layered materials into 2D nanosheets, such as graphene, BN, and MoS<sub>2</sub> due to their simplicity, rapidity, and short reaction time [68,69,88,91]. It has been reported that the as-exfoliated 2D nanosheets can be rolled up into nanoscrolls in order to minimize their surface energy. Therefore, MoS<sub>2</sub> and WS<sub>2</sub> nanoscrolls can be formed by using SCF processing of MoS<sub>2</sub> nanosheets in 30 min, as shown in Figure 7a–g [68,88]. The X-ray diffraction (XRD) patterns of the MoS<sub>2</sub> nanoscrolls clearly show that the surfaces of the MoS<sub>2</sub> nanosheets are not oxidized and are free of impurities [68]. Meanwhile, the lattice structure of the SCF-prepared MoS<sub>2</sub> is essentially unchanged, making this method a convenient and efficient way to prepare nanoscrolls.

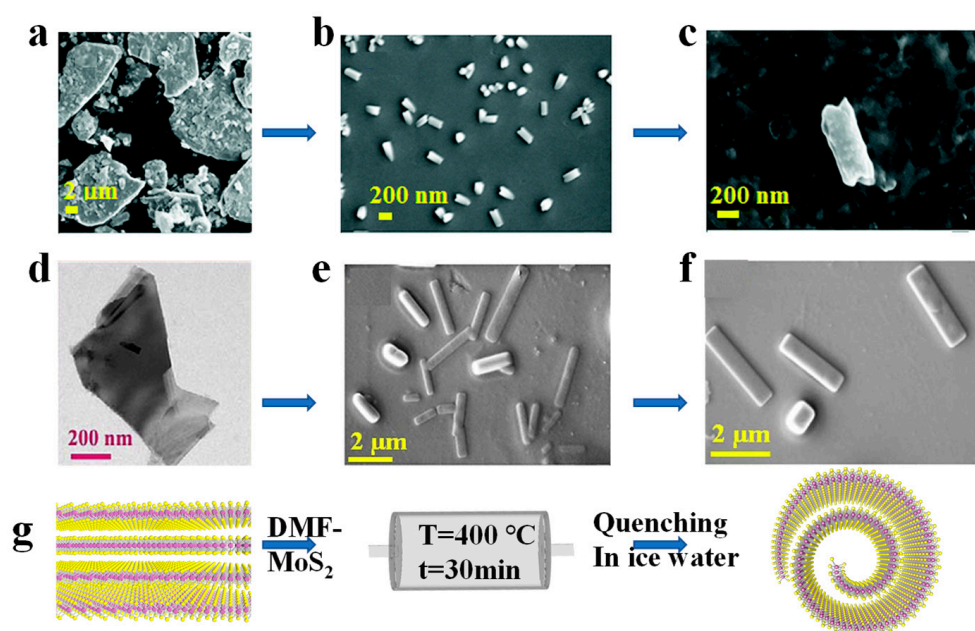


**Figure 7.** Supercritical fluid processing-assisted fabrication of TMDCs nanoscrolls. FE-SEM images of (a) bulk  $\text{MoS}_2$  flake and (b,c) supercritical fluid-prepared  $\text{MoS}_2$  nanoscrolls [88]. FE-SEM images of (d) bulk  $\text{WS}_2$  flake and (e,f) supercritical fluid prepared  $\text{WS}_2$  nanoscrolls; (g) Schematic diagram of supercritical fluid processing-assisted preparation of TMDCs nanoscrolls [68].

### 3.1.6. Shear Force Assisted Fabrication of Nanoscrolls

By using a vortex flow device (VFD),  $\text{MoS}_2$  nanosheets have been successfully transformed into nanoscrolls under continuous flow [50]. In a tilted quartz tube with rapid rotation, a dynamic thin film was generated in VFD, providing mechano-energy as high shear stress during intense micro-mixing. Therefore, the  $\text{MoS}_2$  nanosheets were firstly exfoliated from bulk material due to the strong shear stress. Simultaneously, the as-exfoliated  $\text{MoS}_2$  nanosheets were rolled up in-situ to form scrolls with high yield (Figure 8a,b). At low-speed rotation (4000 rpm), the shear stress is mainly governed by the Typhoon-like toroidal flow, generating centrifugal forces on the tube wall. As a result, the  $\text{MoS}_2$  nanosheets were exfoliated first and then scrolled as the toroidal flow moved upwards (Figure 8c,d) [50,92,93]. As the rotation speed increased to 8000 rpm, the dominated double-helical twisted Faraday wave vortex flow cannot curl and roll up  $\text{MoS}_2$  nanosheets effectively. The morphology of  $\text{MoS}_2$  nanostructure can be changed from lamellae to scroll, by controlling the solvent selection, concentration of bulk material, and the processing parameters of VFD, including rotation speed and rotation angle. The VFD has been widely used to synthesize nanoscrolls from 2D nanosheets, such as graphite, graphene oxide, and hexagonal boron nitride [92–94].

## 3.2. Fabrication of TMDCs Nanoscrolls in Air

### 3.2.1. Plasma-Assisted Fabrication of $\text{MoS}_2$ Nanoscrolls

In 2016, Zhang et al. proposed the preparation of  $\text{MoS}_2$  nanoscrolls by treating CVD-grown monolayer  $\text{MoS}_2$  nanosheets in a weak Ar plasma environment, as shown in Figure 9 [18]. Upon plasma bombardment, the top layer sulfur atoms of the  $\text{MoS}_2$  nanosheets are partially removed as the kinetic energy of  $\text{Ar}^+$  is larger than the binding energy of the Mo-S bond. As a result, the  $\text{MoS}_2$  lattice is disrupted and unsaturated dangling bonds are left, leading to out-of-plane strain. Such kind of strain induces out-of-plane distortion, which rolls up the edge of the  $\text{MoS}_2$  nanosheet to form nanoscrolls [18,58]. The optimum power for fabricating nanoscrolls was 25 W. If the power was too strong, short nanoscrolls were obtained. While a longer time was needed to trigger the scrolling when the power was too weak. When the adjacent edges of  $\text{MoS}_2$  nanosheets are not parallel, a kink will be formed, preventing the formation of a long scroll [18]. In addition,

WS<sub>2</sub> and WSe<sub>2</sub> nanoscrolls were also prepared by treating the monolayer WS<sub>2</sub> and WSe<sub>2</sub> nanosheets in Ar plasma.

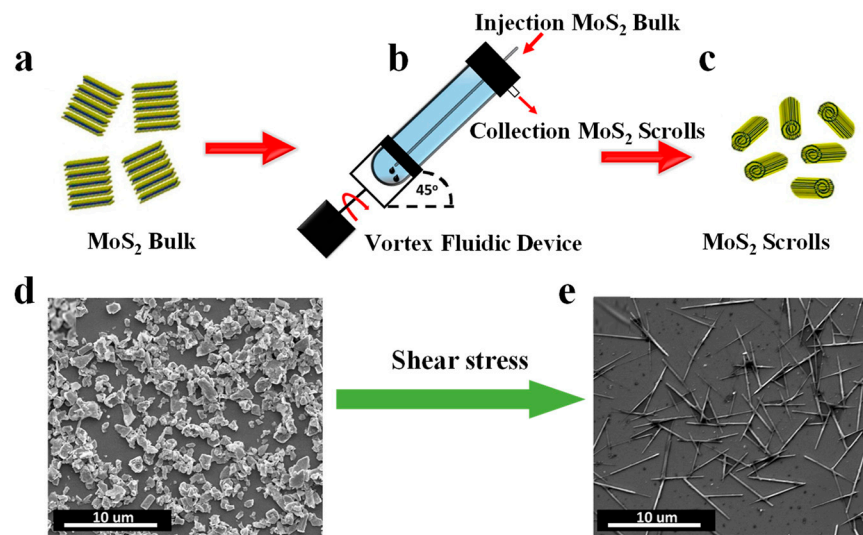


**Figure 8.** Shear force-assisted fabrication of nanoscrolls [50]. (a–c) Schematic illustration of the fabrication of MoS<sub>2</sub> scrolls in VFD. SEM images of the (d) MoS<sub>2</sub> bulk material and (e) as-prepared MoS<sub>2</sub> scrolls in VFD.

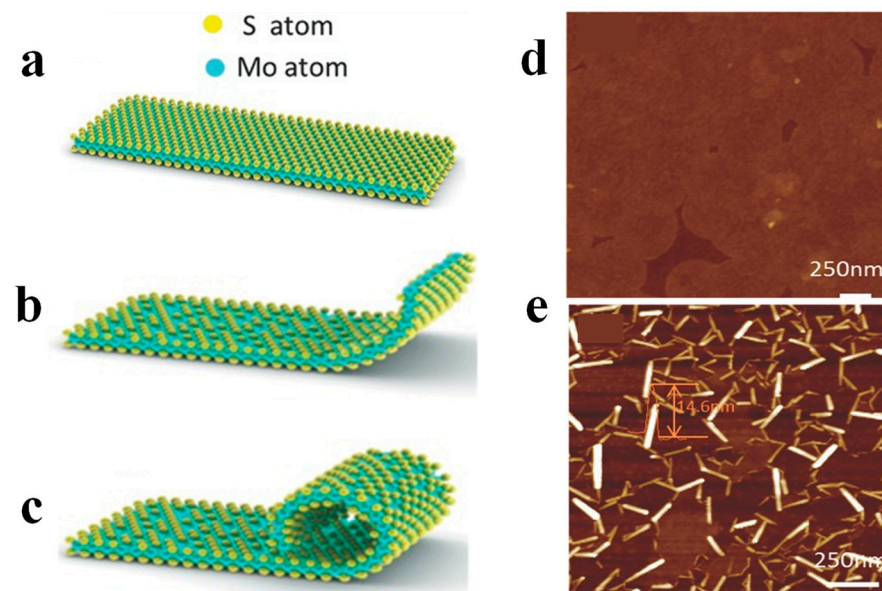


**Figure 9.** Ar plasma-assisted fabrication of MoS<sub>2</sub> nanoscrolls [18]. Schematic structures of (a) monolayer, (b) edge distortion, and (c) scrolled edge of MoS<sub>2</sub> nanosheet under Ar plasma treatment. AFM images of (d) monolayer MoS<sub>2</sub> nanosheet and (e) as-obtained MoS<sub>2</sub> nanoscrolls.

### 3.2.2. Strain-Assisted Fabrication of TMDCs Nanoscrolls

Because of the different thermal expansion coefficients of the MoS<sub>2</sub> and SiO<sub>2</sub>, there are thermal strain gradients between the interface of CVD-grown MoS<sub>2</sub> nanosheets and SiO<sub>2</sub>/Si substrate [58,75,95]. Upon quenching, the orientation-specific fractures are formed on CVD-grown MoS<sub>2</sub> nanosheets due to the existing S vacancies (Figure 10a,b). Since the cooling rate of the top MoS<sub>2</sub> layer is greater than the bottom SiO<sub>2</sub> layer, strong lattice contraction of the MoS<sub>2</sub> layer is observed due to the temperature difference, which induces self-curling at the fractures of the MoS<sub>2</sub> layer (Figure 10c). Afterwards, the curled edge continues to form a scroll in order to minimize the surface energy (Figure 10d).

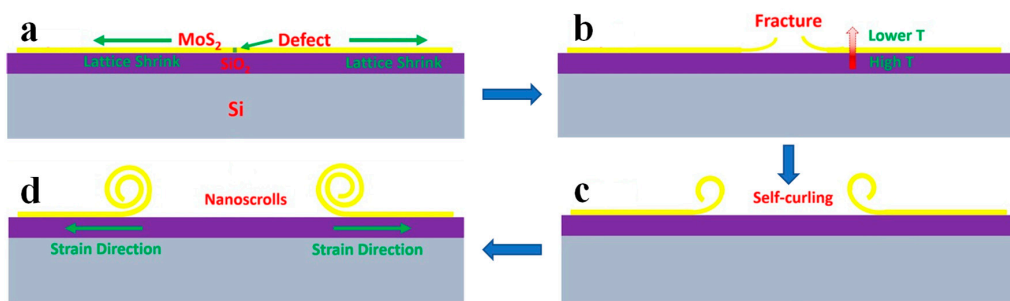


**Figure 10.** Schematic diagram of nanoscroll formed by thermal strain [96]. (a) Monolayer MoS<sub>2</sub> nanosheets were prepared on SiO<sub>2</sub>/Si substrate by CVD. (b) S vacancy acts as crack nuclei due to the thermal strain upon quenching. (c) Self-curling at the fractures of the MoS<sub>2</sub> layer because of the temperature difference between the MoS<sub>2</sub> and SiO<sub>2</sub> layer. (d) The MoS<sub>2</sub> nanoscroll is formed by thermal strain.

Table 1 summarizes the preparation methods of TMDCs nanoscrolls to show the advantages and disadvantages in detail. To date, the TMDCs nanoscrolls have been prepared mainly from CVD-grown monolayer nanosheets or film in large-area. It is known that large-area TMDCs nanosheets can also be obtained by using molecular beam epitaxial (MBE) method and mechanical exfoliation (ME). Therefore, TMDCs nanosheets prepared by the MBE or ME method provide an alternative way for fabricating TMDCs nanoscrolls. Currently, it is difficult to control the geometry of nanoscrolls by using organic or alkaline droplets to directly treat CVD-grown large-area monolayer TMDCs films. In this case, TMDCs nanoscrolls with lengths of several tens to hundreds of micrometers were obtained in random orientation. By using a focused ion beam (FIB), the large-area monolayer TMDCs film can be shaped as long parallel ribbons with controlled width and direction. After dropping the mixture of ethanol and water on these ribbons, long straight TMDCs nanoscrolls can be obtained in array form [24]. The diameter of TMDCs nanoscroll could be tuned by controlling the width of the original ribbon. By using FIB to cut the long TMDCs nanoscrolls, the TMDCs nanoscrolls were patterned into arrays with controlled lengths and locations. By etching the large-area monolayer TMDCs films along the crystalline orientation, TMDCs nanoscrolls arrays with controlled chirality could also be prepared.

**Table 1.** The advantages and disadvantages of preparation methods for TMDCs nanoscrolls.

Methods	Advantages	Challenges	References
In liquid	Solvent evaporation to make nanoscroll	Large area, large size, high productivity, short time consuming, easy to operate	Solvent residue, loose nanoscrolls [22–25,33,53,56,67,70,79,97]
	Alkaline droplet-assisted fabrication of nanoscroll	High yield, high productivity for thick nanosheet	Substrate etching, solvent residue [19,21,26,27,35,51]
	Fabrication of TMDCs nanoscroll by dragging water droplet	High yield, solvent-free residue, tightly packed nanoscroll	Not suitable for water and oxygen-sensitive material [52]
	Amine-functional amphiphilic molecule assisted fabrication of TMDCs nanoscroll	High yield, easy to operate	Small dimension, solvent residue [48,49,82]
	Supercritical fluid-assisted fabrication of nanoscroll	Simple, fast	Small dimension, solvent residue [88]
	Shear force-assisted fabrication of nanoscroll	High productivity, easy to operate	Low proportion of monolayer nanosheet [50]

**Table 1.** Cont.

	Methods	Advantages	Challenges	References
In air	Plasma-assisted fabrication of TMDCs nanoscroll	Simple process, high yield	Small dimension, structural damage	[18,20]
	Strain-assisted fabrication of TMDCs nanoscroll	Simple and repeatable	Complex process, low productivity, incomplete nanoscroll	[17]

#### 4. Applications of TMDCs-NS

##### 4.1. Photodetector Based on TMDCs-NS

Compared to monolayer TMDCs nanosheet, the TMDCs-NS shows much better light absorption efficiency due to its increased thickness of spirally scrolled structure. Thus, the TMDCs-NS should exhibit excellent optoelectronic performance. Recently, the photodetection performance of TMDCs-NS has been investigated [51,98]. Photosensitivity, described by the ratio of photocurrent to dark current (PDR), is one of the most important parameters to evaluate the performance of a photodetector [19,23,35]. Figure 11a shows the PDRs of MoS<sub>2</sub> nanosheet and nanoscroll-based photodetectors under blue light irradiation with a bias voltage of 0.1 V. The PDR of a nanoscroll-based photodetector is about 400, which is about 100 times higher than that of a nanosheet-based one [23]. In addition, the response and recovery time of a nanoscroll-based photodetector is less than the nanosheet-based photodetector. Similar enhanced PDR was also observed in the MoSe<sub>2</sub> nanoscroll-based device [17]. These results indicate that the TMDCs-NS shows much better photodetection performance than the TMDCs nanosheet, which should be attributed to the enhanced light absorption and rapid electron transportation along the 1D structure [24,52]. The photodetection enhancement of TMDCs nanoscrolls could be explained in detail as follows. Firstly, the increased thickness of TMDCs nanoscroll increases the light absorption as the light permeates each layer of the nanoscroll. Although each layer shows low light absorption, the total light absorption of the nanoscroll has increased. Therefore, increased photocurrent is obtained in nanoscroll. In addition, the one-dimensional structure of the nanoscroll confines the electron transportation along the axis direction, and thus rapid electron movement is realized in the nanoscroll compared to that in a 2D nanosheet. Moreover, due to the large surface-to-volume ratio of the MoS<sub>2</sub> nanosheet, the adsorbates, such as O<sub>2</sub> and H<sub>2</sub>O molecules, greatly reduce the photoresponse of the MoS<sub>2</sub> nanosheet-based device. The MoS<sub>2</sub> nanoscroll has a much smaller surface-to-volume ratio than the nanosheet, which can decrease the influence of adsorbates on the photoresponse.

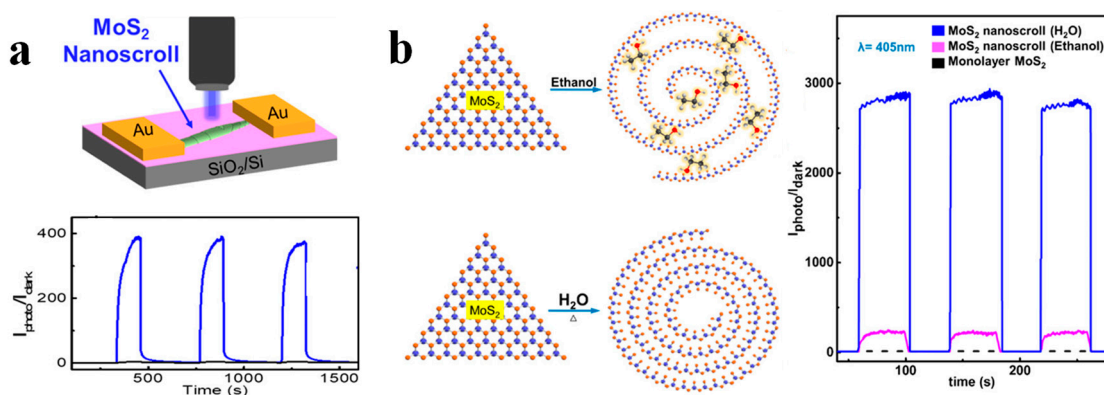


**Figure 11.** Photodetection performance of TMDCs-NS based device. (a) Top panel: Scheme of photodetector based on MoS<sub>2</sub> nanoscroll. Bottom panel: PDR plot of photodetectors based on MoS<sub>2</sub> nanosheet and nanoscroll under 405 nm laser [23]. (b) The scheme of nanoscrolls is made by dropping ethanol and water droplets, respectively. PDR plot of corresponding photodetectors under 405 nm laser [52].

Compared to the  $\text{MoS}_2$  nanoscroll prepared by ethanol droplet ( $\text{MoS}_2$  NS-ethanol), the  $\text{MoS}_2$  nanoscroll prepared by water droplet ( $\text{MoS}_2$  NS-water) shows higher PDR (Figure 11b) [52]. The ethanol molecules trapped in  $\text{MoS}_2$  NS-ethanol reduce the light absorption and hinder the interlayer transport of photogenerated carriers, and thus decrease the photoresponse. In addition, the ethanol can donate an electron to  $\text{MoS}_2$  and thus increase the dark current of  $\text{MoS}_2$  NS-ethanol, which in turn decreases the PDR. Moreover, the  $\text{MoS}_2$  NS-water shows a slightly higher photocurrent than  $\text{MoS}_2$  NS-ethanol.

#### 4.2. Photodetector Based on TMDCs-NS Composite

In bilayer  $\text{WS}_2/\text{MoS}_2$  heterostructure, the carriers can be transferred from  $\text{MoS}_2$  to  $\text{WS}_2$  within 50 fs under illumination, indicating the important role of interface. However, there is only one interface in the bilayer  $\text{WS}_2/\text{MoS}_2$  heterostructure. The photoresponse performance of  $\text{WS}_2/\text{MoS}_2$  heterostructure could be further improved if multiple interfaces can be established. By scrolling the bilayer  $\text{WS}_2/\text{MoS}_2$  heterostructure into  $\text{WS}_2/\text{MoS}_2$  heterostructure nanoscroll, multiple hetero-interfaces are formed, which could show better photoresponse than the bilayer  $\text{WS}_2/\text{MoS}_2$  heterostructure with one hetero-interface. After the bilayer  $\text{WS}_2/\text{MoS}_2$  heterostructure was grown by CVD, the alkaline droplet was dropped on it to roll up the bilayer heterostructure into a nanoscroll [19]. As shown in Figure 12a, the PDR of bilayer  $\text{WS}_2/\text{MoS}_2$  heterostructure-based photodetector is  $\sim 180$  under a blue laser, which is much higher than that of monolayer  $\text{MoS}_2$  or  $\text{WS}_2$  nanosheets. The PDR of  $\text{WS}_2/\text{MoS}_2$  heterostructure nanoscroll-based photodetector is 2700, about an order of magnitude higher than that of bilayer  $\text{WS}_2/\text{MoS}_2$  heterostructure-based photodetector.

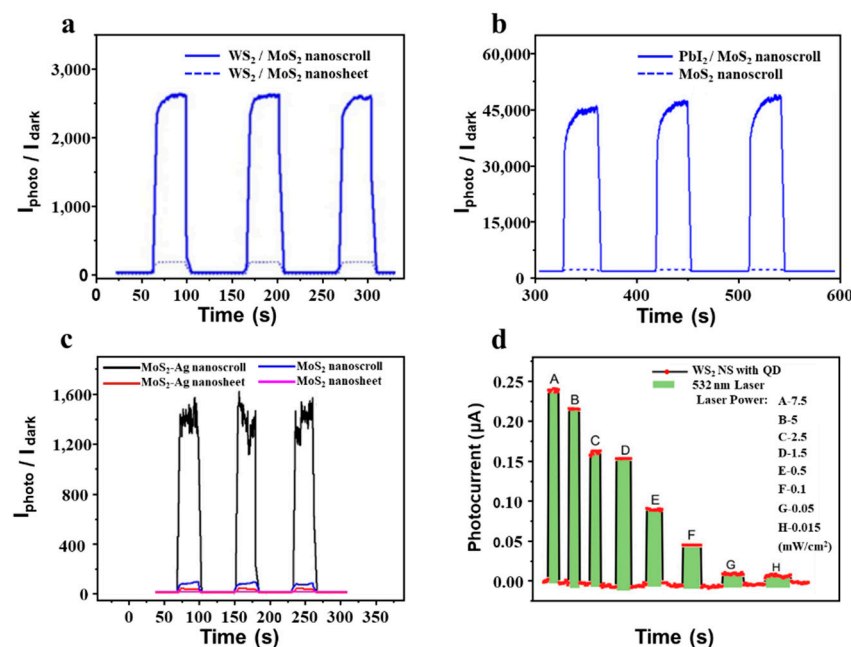


**Figure 12.** Photodetector based on TMDCs-NS composite. (a) Plots of the PDRs of photodetectors based on  $\text{WS}_2/\text{MoS}_2$  nanosheet and nanoscroll under blue laser [19]. (b) PDRs plots of photodetectors based on  $\text{MoS}_2$  nanoscrolls and  $\text{PbI}_2/\text{MoS}_2$  nanoscrolls under 405 nm lasers [51]. (c) Plots of the PDRs of the  $\text{MoS}_2$  nanosheet,  $\text{MoS}_2$  nanoscroll,  $\text{MoS}_2\text{-Ag}$  nanosheet, and  $\text{MoS}_2\text{-Ag}$  NS under a 633 nm laser [35]. (d) Photocurrent variations in hybridized  $\text{WS}_2$  nanoscroll photodetectors under different power densities of a 532 nm laser [79].

By encapsulating photoactive  $\text{PbI}_2$  nanocrystals into  $\text{MoS}_2$  nanoscroll, the PDR of  $\text{MoS}_2$  nanoscroll can be enhanced by two orders of magnitude (Figure 12b) [51]. Similarly, the PDRs of  $\text{MoS}_2$  and  $\text{WS}_2$  nanoscrolls also increased by two orders of magnitude after Ag nanoparticles were trapped in a nanoscroll (Figure 12c) [35]. Moreover, the photoresponsivity of the  $\text{MoS}_2$  nanoscroll was also enhanced by about two orders of mag-

nitude when  $\text{BaTiO}_3$  nanoparticles were encapsulated into it [27]. By doping the  $\text{WS}_2$  nanoscroll with  $\text{CdSe-ZnS}$  quantum dots, the photosensitivity can be enhanced 3000-fold (Figure 12d) [79]. Compared to single TMDCs nanoscrolls, the nanoscroll composite shows excellent photodetection performance [24,70], indicating it could be a promising candidate for high-performance optoelectronics.

#### 4.3. Hydrogen Evolution Reaction

The conductivity and effective active site of the catalyst are two key factors in improving the hydrogen precipitation reaction (HER) [99–101]. TMDCs are considered promising candidates after noble metals for catalytic hydrogen precipitation due to their good electrical conductivity and abundant active edges [66,102,103]. The introduction of a small amount of  $\text{MoS}_x$  greatly enhanced the HER activity of  $\text{NbS}_2$  nanoflakes [100]. The theoretical calculation indicates that Mo edge sites are identified as the catalytically active site for HER [104,105].

A number of efforts have been employed to increase the active sites and conductivity of TMDCs materials [106–108]. Among them, transforming the TMDCs nanosheets into nanoscrolls with active edges is of great interest in electrocatalytic HER [50]. By curling the TMDCs nanosheets to form nanoscrolls, the curled edges provide highly active edge sites for efficient catalysis. Meanwhile, the bending strain of the basal plane also provides more active sites due to the scrolled structure [50,109–111]. In addition, the specific surface area of the nanoscroll increases, converting the solution contact from single-sided contact of the nanosheet to multi-layer contact [112]. As a result, the HER activity of TMDCs-NS is greatly enhanced. Figure 13a shows the polarization curves of metallic  $\text{WSe}_2$  (M- $\text{WSe}_2$ ) and 2H- $\text{WSe}_2$  nanoscrolls compared to the commercial Pt/C catalyst. The M- $\text{WSe}_2$  nanoscroll exhibits higher HER activity, smaller overpotential, and larger current densities than the 2H- $\text{WSe}_2$  nanoscroll, attributed to its good conductivity and enhanced catalytic activity from the scrolled structure [103]. Figure 13b shows the linear scanning voltammogram curves of current density and potential for Pt electrode,  $\text{MoS}_2$  sheet,  $\text{MoS}_2$  nanoscroll,  $\text{MoS}_2$  nanoscrolls@Pt,  $\text{MoS}_2$ @Pt sheet, and  $\text{MoS}_2$ @Pt nanoscroll [48]. The  $\text{MoS}_2$  nanosheet shows overpotential over 400 mV, while that of the  $\text{MoS}_2$  nanoscroll decreases. The overpotential of  $\text{MoS}_2$  nanoscroll decorated by Pt nanoparticles (NPs) greatly decreases, indicating the important role of Pt NPs in enhancing the HER activity. By decorating Pt NPs on  $\text{MoS}_2$  nanosheet ( $\text{MoS}_2$ @Pt sheet), the overpotential further decreases to around 300 mV. After the  $\text{MoS}_2$ @Pt sheet was rolled up to form a  $\text{MoS}_2$ @Pt scroll, the overpotential was reduced to 200 mV, implying the basal plane bending of the nanoscroll can further improve the HER activity.

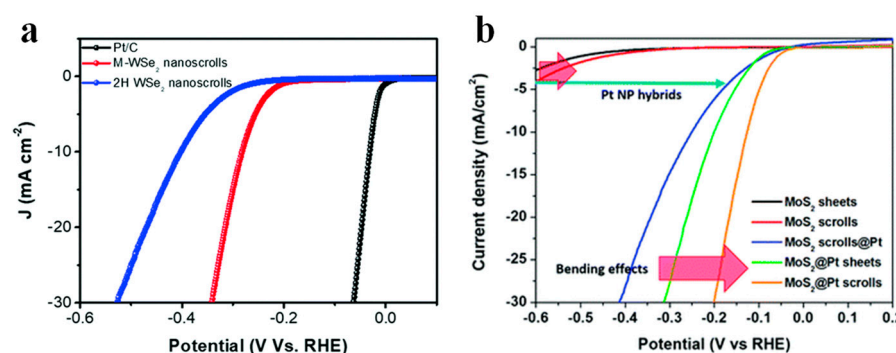


**Figure 13.** Hydrogen evolution reaction (HER) based on TMDCs-NS. (a) HER polarization curves for M- $\text{WSe}_2$  nanoscrolls, 2H- $\text{WSe}_2$  nanoscrolls, and the commercial Pt/C [103]. (b) Polarization curves for Pt electrode,  $\text{MoS}_2$  sheet,  $\text{MoS}_2$  nanoscroll,  $\text{MoS}_2$  nanoscrolls@Pt,  $\text{MoS}_2$ @Pt sheet, and  $\text{MoS}_2$ @Pt nanoscroll [48].

#### 4.4. Gas Sensor

In recent years, TMDCs nanosheets have attracted great attention for gas sensing because of their large surface-to-volume ratio and good electrical properties [113–116]. The TMDCs nanosheet-based gas sensors show high sensitivity for trace gas molecules and good selectivity at room temperature [60,117–119]. However, they suffer from incomplete recovery and poor stability [120], which limit their practical applications. The TMDCs-NS has good conductivity due to its 1D structure and specific surface area from the tubular structure. Meanwhile, the nanoscroll structure also provides tunable space to encapsulate functional nanomaterials for further enhanced performance. Therefore, the TMDCs-NS has been considered to present promising performance in the field of gas sensing [121].

By electrochemically exfoliating InSe crystal in electrolytes containing cetyltrimethylammonium bromide (CTAB), the CTAB-functionalized InSe nanosheets (C-InSe) were obtained [120]. With the aid of solvent evaporation, the C-InSe nanosheets rolled up to form C-InSe nanoscroll. After the as-obtained C-InSe nanoscrolls were deposited on interdigitated electrodes (Figure 14b), they were placed into a chamber with a fixed concentration of NO<sub>2</sub> gas. An LED lamp illuminates light into the chamber through a glass cover (Figure 14a). The response of the C-InSe nanoscrolls-based sensor increases under light illumination (Figure 14c). The enhanced response has arisen from the increased adsorption of NO<sub>2</sub> molecules favored by photogenerated electrons. While desorption of NO<sub>2</sub> is observed as the light intensity increases further, which decreases the response of the sensor. As the concentration of NO<sub>2</sub> increases from 100 ppb to 25 ppm, the response of C-InSe nanosheets and nanoscrolls-based sensors largely increases (Figure 14d). However, the C-InSe nanoscrolls-based sensor exhibits a much better response than the C-InSe nanosheets-based sensor, indicating the superiority of nanoscrolls in gas sensing.

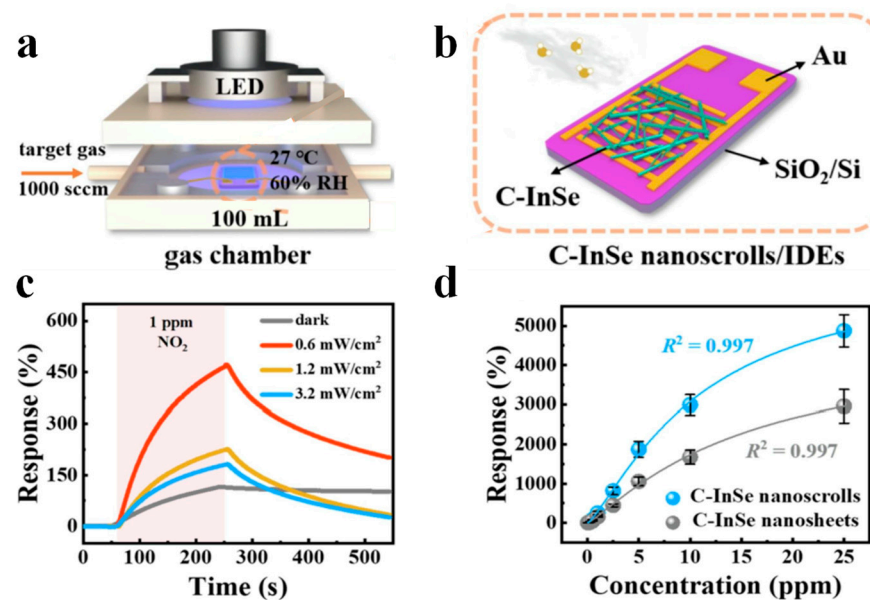


**Figure 14.** Gas sensor based on C-InSe nanoscrolls [120]. **(a,b)** Schematic illustration of C-InSe nanoscroll-based gas sensor and test platform. **(c)** Response curves of C-InSe nanoscrolls sensor towards 1 ppm NO<sub>2</sub> under blue light irradiation with different light intensities. **(d)** Relationship between the response of C-InSe nanosheets and nanoscrolls based sensors and NO<sub>2</sub> concentration.

#### 5. Conclusions

In this review, we summarize a series of fabrication methods of TMDCs nanoscrolls, and briefly demonstrate their applications in photodetection, HER, and gas sensing (Figure 15). Compared to the 2D TMDCs nanosheet, the 1D TMDCs nanoscroll presents higher light absorption efficiency and faster electron transport because of the scrolled structure. Due to their higher specific surface area and active edges, the TMDCs nanoscrolls have shown

excellent performance in catalytic reactions. In conclusion, the TMDCs nanoscrolls are emerging materials with many novel physical and chemical properties that are promising for optoelectronics, catalysis, energy storage, and sensing.

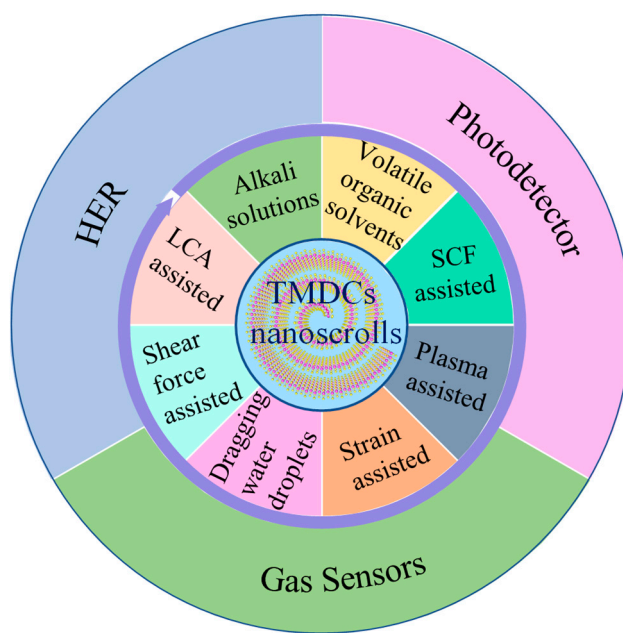


**Figure 15.** Summary of preparation and applications of TMDCs nanoscrolls.

**Author Contributions:** Conceptualization, H.L.; supervision and project administration, H.L.; methodology, H.L., S.Y., P.W. and C.P.; formal analysis, S.Y., P.W., C.P., H.Y., S.W., J.L., H.T. and Z.W.; investigation, S.Y. and P.W.; writing—original draft preparation, H.L., S.Y. and P.W.; revision of the manuscript, H.L. and S.Y. All authors have read and agreed to the published version of the manuscript.

**Funding:** This work was supported by the National Natural Science Foundation of China (Grant No. 51832001 and 21571101), the Natural Science Foundation of Jiangsu Province in China (Grant No. BK20161543), and the Natural Science Foundation of the Jiangsu Higher Education Institutions of China (Grant No. 15KJB430016).

**Institutional Review Board Statement:** Not applicable.

**Informed Consent Statement:** Not applicable.

**Data Availability Statement:** Data can be available upon request from the authors.

**Conflicts of Interest:** The authors declare no conflict of interest.

## References

- Youngblood, N.; Chen, C.; Koester, S.J.; Li, M. Waveguide-integrated black phosphorus photodetector with high responsivity and low dark current. *Nat. Photonics* **2015**, *9*, 247–252. [[CrossRef](#)]
- Wang, F.; Zhang, Y.; Gao, Y.; Luo, P.; Su, J.; Han, W.; Liu, K.; Li, H.; Zhai, T. 2D metal chalcogenides for ir photodetection. *Small* **2019**, *15*, 1901347–1901365. [[CrossRef](#)]
- Wu, Z.; Li, F.; Li, X.; Yang, Y.; Huang, X.; Li, H. Direct synthesis of MoS<sub>2</sub> nanosheets in reduced graphene oxide nanoscroll for enhanced photodetection. *Nanomaterials* **2022**, *12*, 1581. [[CrossRef](#)]
- Andleeb, S.; Wang, X.; Dong, H.; Valligatla, S.; Saggau, C.N.; Ma, L.; Schmidt, O.G.; Zhu, F. Fast-response micro-phototransistor based on MoS<sub>2</sub>/organic molecule heterojunction. *Nanomaterials* **2023**, *13*, 1491. [[CrossRef](#)]
- Al Qaydi, M.; Kotbi, A.; Rajput, N.S.; Bouchalkha, A.; El Marssi, M.; Matras, G.; Kasmi, C.; Jouiad, M. Photodetectionproperties of MoS<sub>2</sub>, WS<sub>2</sub> and Mo<sub>x</sub>W<sub>1-x</sub>S<sub>2</sub> heterostructure: A comparative study. *Nanomaterials* **2022**, *13*, 24. [[CrossRef](#)]
- Yu, X.; Yu, P.; Wu, D.; Singh, B.; Zeng, Q.; Lin, H.; Zhou, W.; Lin, J.; Suenaga, K.; Liu, Z.; et al. Atomically thin noble metal dichalcogenide: A broadband mid-infrared semiconductor. *Nat. Commun.* **2018**, *9*, 1545–1554. [[CrossRef](#)] [[PubMed](#)]

7. Sun, D.; Huang, D.; Wang, H.; Xu, G.-L.; Zhang, X.; Zhang, R.; Tang, Y.; Abd Ei-Hady, D.; Alshitari, W.; Saad Al-Bogami, A.; et al. 1T MoS<sub>2</sub> nanosheets with extraordinary sodium storage properties via thermal-driven ion intercalation assisted exfoliation of bulky MoS<sub>2</sub>. *Nano Energy* **2019**, *61*, 361–369. [[CrossRef](#)]
8. Wang, X.; Li, B.; Bell, D.R.; Li, W.; Zhou, R. Hydrogen and methane storage and release by MoS<sub>2</sub> nanotubes for energy storage. *J. Mater. Chem. A* **2017**, *5*, 23020–23027. [[CrossRef](#)]
9. Jiao, Y.; Hafez, A.M.; Cao, D.; Mukhopadhyay, A.; Ma, Y.; Zhu, H. Metallic MoS<sub>2</sub> for high performance energy storage and energy conversion. *Small* **2018**, *14*, 1800640–1800660. [[CrossRef](#)]
10. Abdolrazzaghan, E.; Zhu, J.; Kim, J.; Yanilmaz, M. MoS<sub>2</sub>-decorated graphene@porous carbon nanofiber anodes via centrifugal spinning. *Nanomaterials* **2022**, *12*, 2505. [[CrossRef](#)]
11. Ali, L.; Subhan, F.; Ayaz, M.; Hassan SS, U.; Byeon, C.C.; Kim, J.S.; Bungau, S. Exfoliation of MoS<sub>2</sub> quantum dots recent progress and challenges. *Nanomaterials* **2022**, *12*, 3465. [[CrossRef](#)] [[PubMed](#)]
12. Anjum, M.A.R.; Jeong, H.Y.; Lee, M.H.; Shin, H.S.; Lee, J.S. Efficient hydrogen evolution reaction catalysis in alkaline media by all-in-one MoS<sub>2</sub> with multifunctional active sites. *Adv. Mater.* **2018**, *30*, 1707105–1707114. [[CrossRef](#)]
13. Duan, H.; Wang, C.; Li, G.; Tan, H.; Hu, W.; Cai, L.; Liu, W.; Li, N.; Ji, Q.; Wang, Y.; et al. Single-atom-layer catalysis in a MoS<sub>2</sub> monolayer activated by long-range ferromagnetism for the hydrogen evolution reaction: Beyond single-atom catalysis. *Angew. Chem. Int. Ed.* **2021**, *60*, 7251–7258. [[CrossRef](#)]
14. Li, G.; Zhang, D.; Yu, Y.; Huang, S.; Yang, W.; Cao, L. Activating MoS<sub>2</sub> for pH-universal hydrogen evolution catalysis. *J. Am. Chem. Soc.* **2017**, *139*, 16194–16200. [[CrossRef](#)]
15. Pan, Y.; Gong, L.; Cheng, X.; Zhou, Y.; Fu, Y.; Feng, J.; Ahmed, H.; Zhang, H. Layer-spacing-enlarged MoS<sub>2</sub> superstructural nanotubes with further enhanced catalysis and immobilization for Li–S batteries. *ACS Nano* **2020**, *14*, 5917–5925. [[CrossRef](#)]
16. Lunardon, M.; Ran, J.; Mosconi, D.; Marega, C.; Wang, Z.; Xia, H.; Agnoli, S.; Granozzi, G. Hybrid transition metal dichalcogenide/graphene microspheres for hydrogen evolution reaction. *Nanomaterials* **2020**, *10*, 2376. [[CrossRef](#)] [[PubMed](#)]
17. Zhou, X.; Tian, Z.; Kim, H.J.; Wang, Y.; Xu, B.; Pan, R.; Chang, Y.J.; Di, Z.; Zhou, P.; Mei, Y. Rolling up MoSe<sub>2</sub> nanomembranes as a sensitive tubular photodetector. *Small* **2019**, *15*, 1902528–1902535. [[CrossRef](#)]
18. Meng, J.; Wang, G.; Li, X.; Lu, X.; Zhang, J.; Yu, H.; Chen, W.; Du, L.; Liao, M.; Zhao, J.; et al. Rolling up a monolayer MoS<sub>2</sub> Sheet. *Small* **2016**, *12*, 3770–3774. [[CrossRef](#)] [[PubMed](#)]
19. Wang, L.; Yue, Q.; Pei, C.; Fan, H.; Dai, J.; Huang, X.; Li, H.; Huang, W. Scrolling bilayer WS<sub>2</sub>/MoS<sub>2</sub> heterostructures for high-performance photo-detection. *Nano Res.* **2020**, *13*, 959–966. [[CrossRef](#)]
20. Chu, X.S.; Li, D.O.; Green, A.A.; Wang, Q.H. Formation of MoO<sub>3</sub> and WO<sub>3</sub> nanoscrolls from MoS<sub>2</sub> and WS<sub>2</sub> with atmospheric air plasma. *J. Mater. Chem. C* **2017**, *5*, 11301–11309. [[CrossRef](#)]
21. Zhao, B.; Wan, Z.; Liu, Y.; Xu, J.; Yang, X.; Shen, D.; Zhang, Z.; Guo, C.; Qian, Q.; Li, J.; et al. High-order superlattices by rolling up van der Waals heterostructures. *Nature* **2021**, *591*, 385–390. [[CrossRef](#)] [[PubMed](#)]
22. Ghosh, R.; Lin, H.-I.; Chen, Y.-S.; Hofmann, M.; Hsieh, Y.-P.; Chen, Y.-F. Efficient light-confinement in heterostructured transition metal dichalcogenide-based nanoscrolls for high-performance photonic devices. *J. Mater. Res.* **2022**, *37*, 660–669. [[CrossRef](#)]
23. Fang, X.; Wei, P.; Wang, L.; Wang, X.; Chen, B.; He, Q.; Yue, Q.; Zhang, J.; Zhao, W.; Wang, J.; et al. Transforming monolayer transition-metal dichalcogenide nanosheets into one-dimensional nanoscrolls with high photosensitivity. *ACS Appl. Mater. Interfaces* **2018**, *10*, 13011–13018. [[CrossRef](#)]
24. Cui, X.; Kong, Z.; Gao, E.; Huang, D.; Hao, Y.; Shen, H.; Di, C.A.; Xu, Z.; Zheng, J.; Zhu, D. Rolling up transition metal dichalcogenide nanoscrolls via one drop of ethanol. *Nat. Commun.* **2018**, *9*, 1301–1308. [[CrossRef](#)] [[PubMed](#)]
25. Deng, W.; You, C.; Chen, X.; Wang, Y.; Li, Y.; Feng, B.; Shi, K.; Chen, Y.; Sun, L.; Zhang, Y. High-performance photodiode based on atomically thin WSe<sub>2</sub> /MoS<sub>2</sub> nanoscroll integration. *Small* **2019**, *15*, 1901544–1901550. [[CrossRef](#)] [[PubMed](#)]
26. Ji, E.; Son, J.; Kim, J.H.; Lee, G.-H. Rolling up two-dimensional sheets into nanoscrolls. *FlatChem* **2018**, *7*, 26–33. [[CrossRef](#)]
27. Su, J.; Li, X.; Xu, M.; Zhang, J.; Liu, X.; Zheng, X.; Shi, Y.; Zhang, Q. Enhancing photodetection ability of MoS<sub>2</sub> nanoscrolls via interface engineering. *ACS Appl. Mater. Interfaces* **2023**, *15*, 3307–3316. [[CrossRef](#)]
28. Du, L.; Hasan, T.; Castellanos-Gomez, A.; Liu, G.-B.; Yao, Y.; Lau, C.N.; Sun, Z. Engineering symmetry breaking in 2D layered materials. *Nat. Rev. Phys.* **2021**, *3*, 193–206. [[CrossRef](#)]
29. Lai, Z.; Chen, Y.; Tan, C.; Zhang, X.; Zhang, H. Self-assembly of two-dimensional nanosheets into one-dimensional nanostructures. *Chem* **2016**, *1*, 59–77. [[CrossRef](#)]
30. Koppens, F.H.; Mueller, T.; Avouris, P.; Ferrari, A.C.; Vitiello, M.S.; Polini, M. Photodetectors based on graphene, other two-dimensional materials and hybrid systems. *Nat. Nanotechnol.* **2014**, *9*, 780–793. [[CrossRef](#)]
31. Long, M.; Wang, P.; Fang, H.; Hu, W. Progress, challenges, and opportunities for 2D material based photodetectors. *Adv. Funct. Mater.* **2018**, *29*, 1803807–1803835. [[CrossRef](#)]
32. Huo, N.; Konstantatos, G. Recent progress and future prospects of 2D-based photodetectors. *Adv. Mater.* **2018**, *30*, 1801164. [[CrossRef](#)]
33. Deng, W.; Chen, X.; Li, Y.; You, C.; Chu, F.; Li, S.; An, B.; Ma, Y.; Liao, L.; Zhang, Y. Strain effect enhanced ultrasensitive MoS<sub>2</sub> nanoscroll avalanche photodetector. *J. Phys. Chem. Lett.* **2020**, *11*, 4490–4497. [[CrossRef](#)] [[PubMed](#)]
34. Tan, C.; Cao, X.; Wu, X.J.; He, Q.; Yang, J.; Zhang, X.; Chen, J.; Zhao, W.; Han, S.; Zhang, H.; et al. Recent advances in ultrathin two-dimensional nanomaterials. *Chem. Rev.* **2017**, *117*, 6225–6331. [[CrossRef](#)] [[PubMed](#)]

35. Yue, Q.; Wang, L.; Fan, H.; Zhao, Y.; Wei, C.; Pei, C.; Song, Q.; Huang, X.; Li, H. Wrapping plasmonic silver nanoparticles inside one-dimensional nanoscrolls of transition-metal dichalcogenides for enhanced photoresponse. *Inorg. Chem.* **2021**, *60*, 4226–4235. [[CrossRef](#)]
36. Hwang, D.Y.; Suh, D.H. Universal surface modification of transition metal dichalcogenide decorated with metal nanoparticles for surface enhanced Raman scattering. *Mater. Res. Bull.* **2017**, *90*, 73–80. [[CrossRef](#)]
37. Perim, E.; Machado, L.D.; Galvao, D.S. A brief review on syntheses, structures, and applications of nanoscrolls. *Front. Mater.* **2014**, *1*, 31–38. [[CrossRef](#)]
38. Costa, M.C.F.; Ng, P.R.; Grebenchuk, S.; Tan, J.Y.; Koon, G.K.W.; Tan, H.L.; Woods, C.R.; Donato, R.K.; Novoselov, K.S.; Neto, A.H.C. Colossal enhancement of electrical and mechanical properties of graphene nanoscrolls. *Carbon* **2023**, *208*, 140–147. [[CrossRef](#)]
39. Muschi, M.; Lalitha, A.; Sene, S.; Aureau, D.; Fregnaux, M.; Esteve, I.; Rivier, L.; Ramsahye, N.; Devautour-Vinot, S.; Sicard, C.; et al. Formation of a single-crystal aluminum-based MOF nanowire with graphene oxide nanoscrolls as structure-directing agents. *Angew. Chem. Int. Ed. Engl.* **2020**, *59*, 10353–10358. [[CrossRef](#)] [[PubMed](#)]
40. Wang, Y.; Jiang, C.; Chen, Q.; Zhou, Q.; Wang, H.; Wan, J.; Ma, L.; Wang, J. Highly promoted carrier mobility and intrinsic stability by rolling up monolayer black phosphorus into nanoscrolls. *J. Phys. Chem. Lett.* **2018**, *9*, 6847–6852. [[CrossRef](#)]
41. Wang, Y.; Tang, X.; Zhou, Q.; Chen, X.; Chen, Q.; Xu, Y. Blue phosphorus nanoscrolls. *Phys. Rev. B* **2020**, *102*, 165428–165434. [[CrossRef](#)]
42. Miranti, R.; Qayyum, M.S.; Sharma, A.; Einarsrud, M.-A.; Mestres, N.; Benelmekki, M. Spectroscopic study of partially oxidized BN nanoscrolls induced by low frequency ultrasonic irradiation. *Appl. Surf. Sci.* **2020**, *515*, 146055–146062. [[CrossRef](#)]
43. Bacon, R. Growth, structure, and properties of graphite whiskers. *J. Appl. Phys.* **1960**, *31*, 283–290. [[CrossRef](#)]
44. Dravid, V.P.; Lin, X.; Wang, Y.; Wang, X.K.; Yee, A.; Ketterson, J.B.; Chang, R.P.H. Buckytubes and derivatives their growth and implications for buckyball formation. *Science* **1993**, *259*, 1601–1604. [[CrossRef](#)] [[PubMed](#)]
45. Shioyama, H.; Akita, T. A new route to carbon nanotubes. *Carbon* **2003**, *41*, 179–198. [[CrossRef](#)]
46. Viculis, L.M.; Mack, J.J.; Kaner, R.B. A chemical route to carbon nanoscrolls. *Science* **2003**, *299*, 1361. [[CrossRef](#)]
47. Braga, S.F.; Coluci, V.R.; Legoa, S.B.; Giro, R.; Galvão, D.S.; Baughman, R.H. Structure and dynamics of carbon nanoscrolls. *Nano Lett.* **2004**, *4*, 881–884. [[CrossRef](#)]
48. Hwang, D.Y.; Choi, K.H.; Park, J.E.; Suh, D.H. Highly efficient hydrogen evolution reaction by strain and phase engineering in composites of Pt and MoS<sub>2</sub> nano-scrolls. *Phys. Chem. Chem. Phys.* **2017**, *19*, 18356–18365. [[CrossRef](#)]
49. Hwang, D.Y.; Choi, K.H.; Park, J.E.; Suh, D.H. Highly thermal-stable paramagnetism by rolling up MoS<sub>2</sub> nanosheets. *Nanoscale* **2017**, *9*, 503–508. [[CrossRef](#)] [[PubMed](#)]
50. Alharbi, T.M.D.; Elmas, S.; Alotabi, A.S.; Andersson, M.R.; Raston, C.L. Continuous flow fabrication of MoS<sub>2</sub> scrolls for electrocatalytic hydrogen evolution. *ACS Sustain. Chem. Eng.* **2022**, *10*, 9325–9333. [[CrossRef](#)]
51. Wu, Z.; Li, F.; Ye, H.; Huang, X.; Li, H. Decorating MoS<sub>2</sub> nanoscrolls with solution-processed PbI<sub>2</sub> nanocrystals for improved photosensitivity. *ACS Appl. Nano Mater.* **2022**, *5*, 15892–15901. [[CrossRef](#)]
52. Zhao, Y.; You, H.; Li, X.; Pei, C.; Huang, X.; Li, H. Solvent-free preparation of closely packed MoS<sub>2</sub> nanoscrolls for improved photosensitivity. *ACS Appl. Mater. Interfaces* **2022**, *14*, 9515–9524. [[CrossRef](#)]
53. Wang, Z.; Wu, H.H.; Li, Q.; Besenbacher, F.; Zeng, X.C.; Dong, M. Self-scrolling MoS<sub>2</sub> metallic wires. *Nanoscale* **2018**, *10*, 18178–18185. [[CrossRef](#)] [[PubMed](#)]
54. Liu, Z.; Gao, J.; Zhang, G.; Cheng, Y.; Zhang, Y.W. From two-dimensional nano-sheets to roll-up structures: Expanding the family of nanoscroll. *Nanotechnology* **2017**, *28*, 385704. [[CrossRef](#)]
55. Taghinejad, H.; Rehn, D.A.; Muccianti, C.; Eftekhar, A.A.; Tian, M.; Fan, T.; Zhang, X.; Meng, Y.; Chen, Y.; Nguyen, T.V.; et al. Defect-mediated alloying of monolayer transition-metal dichalcogenides. *ACS Nano* **2018**, *12*, 12795–12804. [[CrossRef](#)] [[PubMed](#)]
56. Wang, R.; Guo, S.; Li, Z.; Weller, D.; Quan, S.; Yu, J.; Wu, M.; Jiang, J.; Wang, Y.; Liu, R. Strong anisotropic optical properties by rolling up MoS<sub>2</sub> nanoflake. *J. Phys. Chem. Lett.* **2022**, *13*, 8409–8415. [[CrossRef](#)]
57. Chithaiah, P.; Ghosh, S.; Idelevich, A.; Rovinsky, L.; Livneh, T.; Zak, A. Solving the "MoS<sub>2</sub> nanotubes" synthetic enigma and elucidating the route for their catalyst-free and scalable production. *ACS Nano* **2020**, *14*, 3004–3016. [[CrossRef](#)]
58. Han, Y.; Zhou, J.; Dong, J. Electronic and magnetic properties of MoS<sub>2</sub> nanoribbons with sulfur line vacancy defects. *Appl. Surf. Sci.* **2015**, *346*, 470–476. [[CrossRef](#)]
59. Kotekar-Patil, D.; Deng, J.; Wong, S.L.; Lau, C.S.; Goh, K.E.J. Single layer MoS<sub>2</sub> nanoribbon field effect transistor. *Appl. Phys. Lett.* **2019**, *114*, 13508–13513. [[CrossRef](#)]
60. Li, H.; Yin, Z.; He, Q.; Li, H.; Huang, X.; Lu, G.; Fam, D.W.; Tok, A.I.; Zhang, Q.; Zhang, H. Fabrication of single- and multilayer MoS<sub>2</sub> film-based field-effect transistors for sensing NO at room temperature. *Small* **2012**, *8*, 63–67. [[CrossRef](#)] [[PubMed](#)]
61. Mehdizadeh, A.; Zeynali, M.; Karimi, M. Engineering of MoS<sub>2</sub> nanoribbons as high-performance materials for biosensing applications. *Appl. Surf. Sci.* **2021**, *540*, 148349–148359. [[CrossRef](#)]
62. Seravalli, L.; Bosi, M.; Fiorenza, P.; Panasci, S.E.; Orsi, D.; Rotunno, E.; Cristofolini, L.; Rossi, F.; Giannazzo, F.; Fabbri, F. Gold nanoparticle assisted synthesis of MoS<sub>2</sub> monolayers by chemical vapor deposition. *Nanoscale Adv.* **2021**, *3*, 4826–4833. [[CrossRef](#)] [[PubMed](#)]
63. Wang, Q.; Sang, P.; Wei, W.; Li, Y.; Chen, J. Functionalized MoS<sub>2</sub> nanoribbons for intrinsic cold-source transistors: A computational study. *ACS Appl. Nano Mater.* **2022**, *5*, 1178–1184. [[CrossRef](#)]

64. Yi, J.-D.; Liu, T.-T.; Huang, Y.-B.; Cao, R. Solid-state synthesis of MoS<sub>2</sub> nanorod from molybdenum-organic framework for efficient hydrogen evolution reaction. *Sci. China Mater.* **2019**, *62*, 965–972. [CrossRef]
65. Jeong, Y.; Shin, J.; Hong, Y.; Wu, M.; Hong, S.; Kwon, K.C.; Choi, S.; Lee, T.; Jang, H.W.; Lee, J.-H. Gas sensing characteristics of the FET-type gas sensor having inkjet-printed WS<sub>2</sub> sensing layer. *Solid State Electron.* **2019**, *153*, 27–32. [CrossRef]
66. Woods, J.M.; Jung, Y.; Xie, Y.; Liu, W.; Liu, Y.; Wang, H.; Cha, J.J. One-step synthesis of MoS<sub>2</sub>/WS<sub>2</sub> layered heterostructures and catalytic activity of defective transition metal dichalcogenide films. *ACS Nano* **2016**, *10*, 2004–2009. [CrossRef] [PubMed]
67. Lin, C.; Cai, L.; Fu, J.H.; Sattar, S.; Wang, Q.X.; Wan, Y.; Tseng, C.C.; Yang, C.W.; Aljarb, A.; Jiang, K.; et al. Direct band gap in multilayer transition metal dichalcogenide nanoscrolls with enhanced photoluminescence. *ACS Mater. Lett.* **2022**, *4*, 1547–1555. [CrossRef]
68. Thangasamy, P.; Raj, J.A.; Sathish, M. Transformation of multilayer WS<sub>2</sub> nanosheets to 1D luminescent WS<sub>2</sub> nanostructures by one-pot supercritical fluid processing for hydrogen evolution reaction. *Mater. Sci. Semicond. Process.* **2020**, *119*, 105167–105174. [CrossRef]
69. Sathish, M.; Mitani, S.; Tomai, T.; Honma, I. Supercritical fluid assisted synthesis of N-doped graphene nanosheets and their capacitance behavior in ionic liquid and aqueous electrolytes. *J. Mater. Chem. A* **2014**, *2*, 4731–4738. [CrossRef]
70. Zhang, S.; Gao, F.; Feng, W.; Yang, H.; Hu, Y.; Zhang, J.; Xiao, H.; Li, Z.; Hu, P. High-responsivity photodetector based on scrolling monolayer MoS<sub>2</sub> hybridized with carbon quantum dots. *Nanotechnology* **2021**, *33*, 105301–105309. [CrossRef]
71. Xu, J.; Jiang, H.; Shen, Y.; Li, X.Z.; Wang, E.G.; Meng, S. Transparent proton transport through a two-dimensional nanomesh material. *Nat. Commun.* **2019**, *10*, 3971–3979. [CrossRef]
72. Graba, M.; Mamala, J.; Bieniek, A.; Sroka, Z. Impact of the acceleration intensity of a passenger car in a road test on energy consumption. *Energy* **2021**, *226*, 120429–120445. [CrossRef]
73. Yang, J.; Zeng, Z.; Kang, J.; Betzler, S.; Czarnik, C.; Zhang, X.; Ophus, C.; Yu, C.; Bustillo, K.; Pan, M.; et al. Formation of two-dimensional transition metal oxide nanosheets with nanoparticles as intermediates. *Nat. Mater.* **2019**, *18*, 970–976. [CrossRef]
74. Gentile, P.; Cuoco, M.; Volkov, O.M.; Ying, Z.-J.; Vera-Marun, I.J.; Makarov, D.; Ortix, C. Electronic materials with nanoscale curved geometries. *Nat. Electron.* **2022**, *5*, 551–563. [CrossRef]
75. Xu, C.; Wu, X.; Huang, G.; Mei, Y. Rolled-up nanotechnology: Materials issue and geometry capability. *Adv. Mater. Technol.* **2018**, *4*, 1800486–1800512. [CrossRef]
76. Cho, J.H.; Azam, A.; Gracias, D.H. Three dimensional nanofabrication using surface forces. *Langmuir* **2010**, *26*, 16534–16539. [CrossRef]
77. Li, J.; Zhang, J.; Gao, W.; Huang, G.; Di, Z.; Liu, R.; Wang, J.; Mei, Y. Dry-released nanotubes and nanoengines by particle-assisted rolling. *Adv. Mater.* **2013**, *25*, 3715–3721. [CrossRef] [PubMed]
78. Huang, X.; Huang, Z.; Liu, Q.; Zhou, A.a.; Ma, Y.; Wang, J.; Qiu, H.; Bai, H. Organic solvent-assisted lyophilization: A universal method of preparing two-dimensional material nanoscrolls. *ACS Omega* **2019**, *4*, 7420–7427. [CrossRef]
79. Ghosh, R.; Lin, H.I.; Chen, Y.S.; Singh, M.; Yen, Z.L.; Chiu, S.; Lin, H.Y.; Bera, K.P.; Liao, Y.M.; Hofmann, M.; et al. QD/2D hybrid nanoscrolls: A new class of materials for high-performance polarized photodetection and ultralow threshold laser action. *Small* **2020**, *16*, 2003944–2003953. [CrossRef]
80. Na, J.; Park, C.; Lee, C.H.; Choi, W.R.; Choi, S.; Lee, J.-U.; Yang, W.; Cheong, H.; Campbell, E.E.B.; Jhang, S.H. Indirect band gap in scrolled MoS<sub>2</sub> monolayers. *Nanomaterials* **2022**, *12*, 3353. [CrossRef]
81. Taghinejad, H.; Eftekhar, A.A.; Adibi, A. Lateral and vertical heterostructures in twodimensional transition-metal dichalcogenides. *Opt. Mater. Express* **2019**, *9*, 1590–1607. [CrossRef]
82. Hwang, D.Y.; Choi, K.H.; Suh, D.H. A vacancy-driven phase transition in MoX<sub>2</sub> (X: S, Se and Te) nanoscrolls. *Nanoscale* **2018**, *10*, 7918–7926. [CrossRef] [PubMed]
83. Hwang, D.Y.; Suh, D.H. Evolution of a high local strain in rolling up MoS<sub>2</sub> sheets decorated with Ag and Au nanoparticles for surface-enhanced Raman scattering. *Nanotechnology* **2017**, *28*, 25603–25614. [CrossRef] [PubMed]
84. Reddy, J.; Basha, H.G.; Narayanan, N.S.V. Heat flow visualization of a chemical compound isobutane (C<sub>4</sub>H<sub>10</sub>) past a vertical cylinder in the subcritical, near critical and supercritical regions. *J. Mol. Struct.* **2018**, *259*, 209–219. [CrossRef]
85. El Khouri, L.; Carle's, P. Supercritical fluids as experimental models for geophysical flows. *Int. J. Thermophys.* **2003**, *24*, 683–693. [CrossRef]
86. Shah, P.S.; Hanrath, T.; Johnston, K.P.; Korgel, B.A. Nanocrystal and nanowire synthesis and dispersibility in supercritical fluids. *J. Phys. Chem. B* **2004**, *108*, 9574–9587. [CrossRef]
87. Schienbein, P.; Marx, D. Assessing the properties of supercritical water in terms of structural dynamics and electronic polarization effects. *Phys. Chem. Chem. Phys.* **2020**, *22*, 10462–10479. [CrossRef]
88. Thangasamy, P.; Sathish, M. Rapid, one-pot synthesis of luminescent MoS<sub>2</sub> nanoscrolls using supercritical fluid processing. *J. Mater. Chem. C* **2016**, *4*, 1165–1169. [CrossRef]
89. Thangasamy, P.; Sathish, M. Supercritical fluid processing: A rapid, one-pot exfoliation process for the production of surfactant-free hexagonal boron nitride nanosheets. *CrystEngComm* **2015**, *17*, 5895–5899. [CrossRef]
90. Wang, W.; Gai, Y.; Xiao, D.; Zhao, Y. A facile and general approach for production of nanoscrolls with high-yield from two-dimensional nanosheets. *Sci. Rep.* **2018**, *8*, 15262–15268. [CrossRef]

91. Rangappa, D.; Sone, K.; Wang, M.; Gautam, U.K.; Golberg, D.; Itoh, H.; Ichihara, M.; Honma, I. Rapid and direct conversion of graphite crystals into high-yielding, good-quality graphene by supercritical fluid exfoliation. *Chem. Eur. J.* **2010**, *16*, 6488–6494. [[CrossRef](#)]
92. Alharbi, T.M.D.; Jellicoe, M.; Luo, X.; Vimalanathan, K.; Alsulami, I.K.; Al Harbi, B.S.; Igder, A.; Alrashaidi, F.A.J.; Chen, X.; Stubbs, K.A.; et al. Sub-micron moulding topological mass transport regimes in angled vortex fluidic flow. *Nanoscale Adv.* **2021**, *3*, 3064–3075. [[CrossRef](#)] [[PubMed](#)]
93. Vimalanathan, K.; Suarez-Martinez, I.; Peiris, M.C.R.; Antonio, J.; de Tomas, C.; Zou, Y.; Zou, J.; Duan, X.; Lamb, R.N.; Harvey, D.P.; et al. Vortex fluidic mediated transformation of graphite into highly conducting graphene scrolls. *Nanoscale Adv.* **2019**, *1*, 2495–2501. [[CrossRef](#)]
94. Al-Antaki, A.H.M.; Luo, X.; Alharbi, T.M.D.; Harvey, D.P.; Pye, S.; Zou, J.; Lawrance, W.; Raston, C.L. Inverted vortex fluidic exfoliation and scrolling of hexagonal-boron nitride. *RSC Adv.* **2019**, *9*, 22074–22079. [[CrossRef](#)]
95. Huang, G.; Mei, Y. Thinning and shaping solid films into functional and integrative nanomembranes. *Adv. Mater.* **2012**, *24*, 2517–2546. [[CrossRef](#)] [[PubMed](#)]
96. Hao, S.; Yang, B.; Gao, Y. Fracture-induced nanoscrolls from CVD-grown monolayer molybdenum disulfide. *Phys. Status Solidi Rapid Res. Lett.* **2016**, *10*, 549–553. [[CrossRef](#)]
97. Qian, Q.; Zu, R.; Ji, Q.; Jung, G.S.; Zhang, K.; Zhang, Y.; Buehler, M.J.; Kong, J.; Gopalan, V.; Huang, S. Chirality-dependent second harmonic generation of MoS<sub>2</sub> nanoscroll with enhanced efficiency. *ACS Nano* **2020**, *14*, 13333–13342. [[CrossRef](#)] [[PubMed](#)]
98. Fan, X.; Su, L.; Zhang, F.; Huang, D.; Sang, D.K.; Chen, Y.; Li, Y.; Liu, F.; Li, J.; Zhang, H.; et al. Layer-dependent properties of ultrathin ges nanosheets and application in uv-vis photodetectors. *ACS Appl. Mater. Interfaces* **2019**, *11*, 47197–47206. [[CrossRef](#)]
99. Morales-Guio, C.G.; Sterna, L.-A.; Hu, X. Nanostructured hydrotreating catalysts for electrochemical hydrogen evolution. *Chem. Soc. Rev.* **2014**, *43*, 6555–6569. [[CrossRef](#)]
100. Zhou, X.; Lin, S.H.; Yang, X.; Li, H.; Hedhili, M.N.; Li, L.J.; Zhang, W.; Shi, Y. MoS<sub>x</sub>-coated NbS<sub>2</sub> nanoflakes grown on glass carbon: An advanced electrocatalyst for the hydrogen evolution reaction. *Nanoscale* **2018**, *10*, 3444–3450. [[CrossRef](#)]
101. Li, H.; Jia, X.; Zhang, Q.; Wang, X. Metallic transition-metal dichalcogenide nanocatalysts for energy conversion. *Chem* **2018**, *4*, 1510–1537. [[CrossRef](#)]
102. Mattinen, M.; Leskelä, M.; Ritala, M. Atomic layer deposition of 2D metal dichalcogenides for electronics, catalysis, energy storage, and beyond. *Adv. Mater. Interfaces* **2021**, *8*, 2001677–2001724. [[CrossRef](#)]
103. Wang, W.; Li, Y.; Li, M.; Shen, H.; Zhang, W.; Zhang, J.; Liu, T.; Kong, X.; Bi, H. Metallic phase WSe<sub>2</sub> nanoscrolls for the hydrogen evolution reaction. *New J. Chem.* **2022**, *46*, 8381–8384. [[CrossRef](#)]
104. Hinnemann, B.; Moses, P.G.; Bonde, J.; Jørgensen, K.P.; Nielsen, J.H.; Horch, S.; Chorkendorff, I.; Nørskov, J.K. Biomimetic hydrogen evolution: MoS<sub>2</sub> nanoparticles as catalyst for hydrogen evolution. *J. Am. Chem. Soc.* **2005**, *127*, 5308–5309. [[CrossRef](#)] [[PubMed](#)]
105. Wang, F.; Shifa, T.A.; Zhan, X.; Huang, Y.; Liu, K.; Cheng, Z.; Jiang, C.; He, J. Recent advances in transition-metal dichalcogenide based nanomaterials for water splitting. *Nanoscale* **2015**, *7*, 19764–19788. [[CrossRef](#)] [[PubMed](#)]
106. Jaramillo, T.F.; Jørgensen, K.P.; Bonde, J.; Nielsen, J.H.; Horch, S.; Chorkendorff, I. Identification of active edge sites for electrochemical H<sub>2</sub> evolution from MoS<sub>2</sub> nanocatalysts. *Science* **2007**, *317*, 100–102. [[CrossRef](#)]
107. Yan, Y.; Xia, B.; Xu, Z.; Wang, X. Recent development of molybdenum sulfides as advanced electrocatalysts for hydrogen evolution reaction. *ACS Catal.* **2014**, *4*, 1693–1705. [[CrossRef](#)]
108. Henckel, D.A.; Lenz, O.M.; Krishnan, K.M.; Cossairt, B.M. Improved HER catalysis through facile, aqueous electrochemical activation of nanoscale WSe<sub>2</sub>. *Nano Lett.* **2018**, *18*, 2329–2335. [[CrossRef](#)]
109. Voiry, D.; Yang, J.; Chhowalla, M. Recent strategies for improving the catalytic activity of 2D TMD nanosheets toward the hydrogen evolution reaction. *Adv. Mater.* **2016**, *28*, 6197–6206. [[CrossRef](#)] [[PubMed](#)]
110. Lu, Q.; Yu, Y.; Ma, Q.; Chen, B.; Zhang, H. 2D transition-metal-dichalcogenide-nanosheet-based composites for photocatalytic and electrocatalytic hydrogen evolution reactions. *Adv. Mater.* **2016**, *28*, 1917–1933. [[CrossRef](#)] [[PubMed](#)]
111. Yuan, J.; Wu, J.; Hardy, W.J.; Loya, P.; Lou, M.; Yang, Y.; Najmaei, S.; Jiang, M.; Qin, F.; Keyshar, K.; et al. Facile synthesis of single crystal vanadium disulfide nanosheets by chemical vapor deposition for efficient hydrogen evolution reaction. *Adv. Mater.* **2015**, *27*, 5605–5609. [[CrossRef](#)] [[PubMed](#)]
112. Jiang, Z.; Zhou, W.; Hu, C.; Luo, X.; Zeng, W.; Gong, X.; Yang, Y.; Yu, T.; Lei, W.; Yuan, C. Interlayer-confined NiFe dual atoms withinMoS<sub>2</sub> electrocatalyst for ultra-efficient acidic overall water splitting. *Adv. Mater.* **2023**, *35*, 2300505. [[CrossRef](#)] [[PubMed](#)]
113. Kim, R.; Jang, J.-S.; Kim, D.-H.; Kang, J.-Y.; Cho, H.-J.; Jeong, Y.J.; Kim, I.-D. A general synthesis of crumpled metal oxide nanosheets as superior chemiresistive. *Adv. Funct. Mater.* **2019**, *29*, 1903128. [[CrossRef](#)]
114. Bag, A.; Lee, N.-E. Gas sensing with heterostructures based on two-dimensional nanostructured materials a review. *J. Mater. Chem. C* **2019**, *7*, 13367–13383. [[CrossRef](#)]
115. Kumar, R.; Goel, N.; Hojaberdiiev, M.; Kumar, M. Transition metal dichalcogenides-based flexible gas sensors. *Sens. Actuator A Phys.* **2020**, *303*, 111875–111902. [[CrossRef](#)]
116. Goswami, P.; Gupta, G. Recent progress of flexible NO<sub>2</sub> and NH<sub>3</sub> gas sensors based on transition metal dichalcogenides for room temperature sensing. *Mater. Today Chem.* **2022**, *23*, 100726–100739. [[CrossRef](#)]
117. Liu, J.; Hu, Z.; Zhang, Y.; Li, H.Y.; Gao, N.; Tian, Z.; Zhou, L.; Zhang, B.; Tang, J.; Zhang, J.; et al. MoS<sub>2</sub> nanosheets sensitized with quantum dots for room-temperature gas sensors. *Nano-Micro Lett.* **2020**, *12*, 59–72. [[CrossRef](#)]

118. Bharathi, P.; Harish, S.; Shimomura, M.; Ponnusamy, S.; Mohan, M.K.; Archana, J.; Navaneethan, M. Conductometric NO<sub>2</sub> gas sensor based on Co-incorporated MoS<sub>2</sub> nanosheets for room temperature applications. *Sens. Actuators B Chem.* **2022**, *360*, 131600. [[CrossRef](#)]
119. Bai, H.; Guo, H.; Feng, C.; Wang, J.; Liu, B.; Xie, Z.; Guo, F.; Chen, D.; Zhang, R.; Zheng, Y. Light-activated ultrasensitive NO<sub>2</sub> gas sensor based on heterojunctions of CuO nanospheres/MoS<sub>2</sub> nanosheets at room temperature. *Sens. Actuators B Chem.* **2022**, *368*, 132131–132146. [[CrossRef](#)]
120. Zhang, L.; Hao, Q.; Liu, J.; Zhou, J.; Zhang, W.; Li, Y. Rolling up of 2D nanosheets into 1D Nanoscrolls: Visible-light-activated chemiresistors based on surface modified indium selenide with enhanced sensitivity and stability. *Chem. Eng. J.* **2022**, *446*, 136937. [[CrossRef](#)]
121. Park, H.; Park, J.; Kang, S.-W.; Jeong, S.-H. 3D-nanostructured MoS<sub>2</sub> nanoscroll with highly active sites for improving NO<sub>2</sub> gas detection. *Mater. Lett.* **2023**, *349*, 134733–134737. [[CrossRef](#)]

**Disclaimer/Publisher’s Note:** The statements, opinions and data contained in all publications are solely those of the individual author(s) and contributor(s) and not of MDPI and/or the editor(s). MDPI and/or the editor(s) disclaim responsibility for any injury to people or property resulting from any ideas, methods, instructions or products referred to in the content.